



14-16 September, 2022
Ashtarak, Armenia



International Conference

Laser Physics 2022

Book of Abstracts



Ministry of Education, Science,
Culture and Sports RA
Science Committee

OPTICA | Formerly
OSA
IPR Armenia Student Chapter

The goal of “Laser Physics 2022” is to bring together a multi-disciplinary group of scientists and engineers from different countries to present and exchange breakthrough ideas relating to Lasers, Optics and Photonics.

TOPICS

- ✦ Lasers, New Laser Technologies and Applications
- ✦ Optical and Scintillating Materials, Characterization Methods and Techniques
- ✦ Light-Matter Interaction, Including Resonant Interaction with Atoms
- ✦ Laser-Assisted Surface Effects
- ✦ Nonlinear Optics and Novel Phenomena
- ✦ Laser Spectroscopy, Ultrafast Phenomena and Mathematical Modelling
- ✦ Physical Optics, Atomic Physics, Singular Optics
- ✦ Optical Magnetometry
- ✦ Quantum Optics and Matter Waves
- ✦ Quantum Information
- ✦ Optical Properties of Structured Media, Micro and Nano-Optics
- ✦ Optoelectronics
- ✦ Photonics, Photonic Systems, Biophotonics
- ✦ Optical Sensors
- ✦ Graphene for Photonics
- ✦ Holography and Imaging

CONFERENCE INTERNATIONAL ADVISORY BOARD

- ✦ Charles Adams (Durham University, UK)
- ✦ Marcis Auzinsh (University of Latvia, LV)
- ✦ Dmitry Budker (JGU Mainz, DE)
- ✦ Christophe Dujardin (Institut Lumière Matière, FR)
- ✦ Klass Bergmann (Technical University Kaiserslautern, DE)
- ✦ Ron Folman (Ben-Gurion University of the Negev, IL)
- ✦ Wojciech Gawlik (Jagiellonian University, PL)
- ✦ Yuri Kivshar (The Australian National University, AU)
- ✦ Claude Leroy (Laboratoire Interdisciplinaire Carnot de Bourgogne, FR)
- ✦ Goran Pichler (Institute of Physics, Zagreb, Croatia)
- ✦ Emilio Mariotti (University of Siena, Siena, Italy)
- ✦ Tigran Vartanyan (ITMO University, RU)
- ✦ Gagik Gurzadyan (Dalian University of Technology, PRC)

SCIENTIFIC/PROGRAMME COMMITTEE

- ✦ Rafael Drampyan (IPR) — Chairman
- ✦ David Sarkisyan (IPR)
- ✦ Pavel Muzhikyan (IPR)
- ✦ Gayane Grigoryan (IPR)
- ✦ Artur Ishkhanyan (IPR)
- ✦ Edvard Kokanyan (IPR)
- ✦ Radik Kostanyan (IPR)
- ✦ Armen Melikyan (Russian-Armenian University)
- ✦ Atom Muradyan (Yerevan State University)
- ✦ Roman Allahverdyan (Yerevan State University)
- ✦ Aram Papoyan (IPR)
- ✦ Ashot Petrosyan (IPR)

LOCAL ORGANIZING COMMITTEE

- ✦ Emil Gazazyan (IPR) (conference scientific secretary)
- ✦ Pavel Muzhikyan (IPR)
- ✦ Paytsar Mantashyan (IPR)
- ✦ Lusine Tsarukyan (IPR)
- ✦ Gayane Chilingaryan (IPR)
- ✦ Astghik Ghazaryan (IPR)
- ✦ Ariga Arakelyan (IPR)
- ✦ Vardges Avagyan (IPR)

CO-ORGANIZING STUDENT PROJECT

- ✦ IPR Armenia OPTICA Student Chapter

SPONSORS

The conference was sponsored by Science Committee of Armenia. “IPR Armenia” Optica Student Chapter sponsors the Best Student Presentation Award.



Ministry of Education, Science,
Culture and Sports RA
Science Committee





International Conference

Laser Physics 2022

Abstracts from 14-16 September, 2022

*Abstracts of
Plenary Reports*

Plenary report

Massive Matter-Wave Interferometers on the Atom Chip with Nano-Diamonds: a Roadmap

R. Folman

Ben-Gurion University of the Negev, Beer Sheva, Israel

Email: folman@bgu.ac.il

Matter-wave interferometry provides an excellent tool for fundamental studies as well as technological applications. Looking to the future, a spatial superposition of massive objects has long been sought after due to the potential for new insight into the foundations of quantum mechanics (QM), the interface of QM and gravity, and as a tool for testing exotic theories. In our group, several interferometry experiments have been conducted with a BEC on an atom chip. I will briefly present realized interferometric schemes based on Stern-Gerlach interferometry (SGI), and mainly focus on plans to use this unique SGI to put a nano diamond in a state of spatial superposition.

Plenary report

Recent Progress in the Development of Electrically Controllable Lenses and their Applications

Z. Zemska¹, P. Larochelle¹, T. Galstian^{1,2,3}

¹ *Université Laval, 2375 rue de la Terrasse, Québec, QC, Canada, G1V0A6.*

² *PATQER photonique inc.*

³ *TLCL Optical Research or LensVector inc.*

Email: galstian@phy.ulaval.ca

Optical systems are becoming more miniaturized, integrated and specialized. This increases the complexity of their manufacturing as well as their sensitivity to operation conditions. For example, exposition of the device to increased temperature may dramatically affect its performance. The integration of electrically adjustable components (such as lenses) may be very beneficial here since it will allow the dynamic adjustment and optimization of the device operations. Electrically tunable liquid crystal lenses have attracted significant attention in the past thanks to their low power consumption, small size and the relative ease of manufacturing. Such applications, as auto-focus in cell phone cameras, have been demonstrated successfully. However, some difficulties remained for their manufacturing due to the use of semiconductor layers.

In the present work, we shall describe some examples of needs and briefly introduce liquid crystal optics. Then we shall describe several ways of creating electrically tunable lenses, their advantages and drawbacks. Finally, we shall describe the most recent generation of tunable lenses, we have developed, where the semiconductor layers are replaced by a simple indium tin oxide pattern (Fig.1). This allows easier fabrication of lenses but also procures

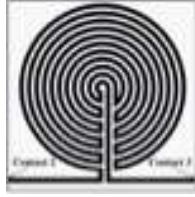


Fig.1. Schematic demonstration of a pattern of a transparent indium tin oxide electrode used for tunable lens fabrication (from).

environmental (thermal) stability during the lens operation. We shall briefly describe few new applications that become possible with this type of lenses.

References

- [1] Galstian, T.V., “Smart mini-cameras”. CRC Press. 2013.
- [2] T. Galstian, K. Asatryan, V. Presniakov, A. Zohrabyan, A. Tork, A. Bagramyan, S. Careau, M. Thiboutot, M. Cotovanu, *Optics Letters*, **41**, [Issue 14](#), p. 3265 (2016).
- [3] Z. Zemska and T. Galstian, *Electrically tunable lens with non-monotonic wavefront control capability*, Accepted in *Optics Letters*.

Plenary report

Photoionization of Silver: Spectroscopic Research and Application to Radiopharmacy in the SPES – IsolPharm Project Context

E. Mariotti¹, A. Arzenton^{1,2}, S. Farracane², A. Khanbekyan¹, O.S. Kwairakpam^{1,2},
P. Nicolosi³, D. Scarpa², A. Andrighetto²

¹ DSFTA - Università di Siena, via Roma 56, Siena, INFN – sezione di Pisa

² INFN – Laboratori Nazionali di Legnaro, viale dell’Università 2, 35020 Legnaro (PD)

³ DEI – Università di Padova, LUXOR CNR IFN - Via Trasea 7, 35131 Padova

Email: emilio.mariotti@unisi.it

Laser Resonant photo-ionization technique is the best tool for selective production of elements in an ISOL facility. A specific atomic species is excited with photons of precise wavelengths, which correspond to the electronic transitions particular to one element, in such a way that photo-ionization can be achieved. Owing to its high selectivity, laser ion sources are employed in most radio-active beam facilities.

SPES project, under INFN-LNL, is constructing a second-generation ISOL facility planned to be online by 2025. A proton beam @40 MeV will be irradiated on a UCx target, which will produce hundreds of isotopes of various elements through nuclear reactions. The laser ion source can selectively ionize an element of interest from this huge range of elements. Coupled to a mass separator, the system can efficiently provide specific isotopes. ISOLPHARM is a branch of the SPES project which concerns the medical application of radio-nuclides. ¹¹¹Ag is an isotope of great interest

for ISOLPHARM and so there is a strong motivation to understand its possible photo-ionization schemes and, among them, the most efficient one. Offline studies of the Ag schemes are being performed using diagnostic tools such as Hollow Cathode Lamp (HCL) and Time of Flight Mass Spectrometer (TOFMS) in the SPES offline laser lab.

Interesting results have been observed during these studies. Opto galvanic effect has been observed in the HCL when injected with lasers of 328.163nm and 421.212nm. Wavelength scans with the mentioned wavelengths as central value shows clear indication of resonance with linewidths of few pm. The photo-ionization signal has been detected in the ToF-MS system too. Apart from clear indication of laser resonance, isotopic separation of natural Ag [Ag107 (51.83%) and Ag109 (48.17%)] has been clearly observed.

*Abstracts of
Invited Reports*

Invited report

A new Level-Crossing Two-State Model Solvable in Terms of Hypergeometric Functions

T. A. Shahverdyan, T. A. Ishkhanyan, and A. M. Ishkhanyan

Institute for Physical Research, Ashtarak, 0203 Armenia

Email: aishkhanyan@gmail.com

We present a new exactly integrable time-dependent constant-amplitude level-crossing two-state quantum model for which the detuning of the excitation laser field varies with time over a restricted interval. This field configuration is a member of one of the eleven independent classes of general Heun two-state models. We prove that this is the only non-classical *unconditionally* solvable field configuration among the general Heun classes, solvable in terms of finite sums of Gauss hypergeometric functions. Each of the two fundamental solutions that compose the general solution of the problem is written as an irreducible linear combination of two ordinary hypergeometric functions.

Invited report

The Gauge Degrees of Freedom in the Theory of the Massless Spin 2 Particle, Solutions with Spherical Symmetry

A. V. Bury¹, A. V. Ivashkevich¹, A. V. Chichurin², V. M. Red'kov^{1g}

¹ *B.I. Stepanov Institute of Physics, 68 Independence ave. 220072 Minsk*

² *Institute of Mathematics and Computer Science,*

The John Paul II Catholic University of Lublin, Lublin, Poland 20-708

Email: v.redkov@ifanbel.bas-net.by

The matrix equation for a massless spin 2 particle is considered with the use of the tetrad formalism in the spherical coordinates of Minkowski space. The separation of the variables is done, the problem reduces to 11 differential second order equations related to the scalar and symmetric tensor. The simple 11-component solution Ψ_1 of this radial system related to spacial parity $P = (-1)^{j+1}$ has been constructed in terms of Bessel functions.

The four gauge solutions, Φ_i , $i = 1, 2, 3, 4$ or massless spin 2 field have been found in explicit form. Such gauge solutions do not contribute into physically observable quantities like energy-momentum tensor. They are derived according to Pauli – Fierz theory from 4 independent spherical solutions for a spin 1 massless particle. We prove that the simple solution Ψ_1 cannot be presented as a linear combination of 4 gauge solutions Φ_i , $i = 1, 2, 3, 4$. Therefore, these gauge solutions are to be found and eliminated from solutions of the radial system for spin 2 field (8 second order differential equations, related to states with opposite parity $P = (-1)^{j+1}$).

The structure of 4 gauge solutions permits us to propose the general substitutions for 8 unknown

variables in the form of linear combinations of 5 Bessel functions with different indices. These substitutions in general contain 40 unknown numerical coefficients. With the use of the properties of Bessel functions, we can reduce the problem to the homogeneous algebraic linear system of 40 equations. We may expect existence of 5 independent solutions. After eliminating the four gauge solutions, we should obtain one solution Ψ_2 , additional to Ψ_1 , which does not contain any gauge constituents.

Invited report

Electromagnetically Induced Transparency Effect Using Magnetically Induced Transitions: Circular Dichroism Manifestation

D. Sarkisyan, A. Tonoyan, and A. Sargsyan

Institute for Physical Research, National Academy of Sciences of Armenia, Ashtarak, 0203 Armenia

Email: sarkdav@gmail.com

Magnetically induced (MI) transitions $F_g = 1 \rightarrow F_e = 3$ of the ^{87}Rb , ^{39}K and Na D₂ line as well as $F_g = 2 \rightarrow F_e = 4$ of the ^{85}Rb D₂ line and $F_g = 4 \rightarrow F_e = 2$, $F_g = 3 \rightarrow F_e = 5$ of the Cs atoms D₂ line using the σ^+ and σ^- circularly polarized radiation and can be successfully implemented to form optical EIT-resonances in strong magnetic fields up to a few kG under electromagnetically induced transparency (EIT) conditions. For this purpose it is convenient to use 1.5- μm -thick cell filled with Rb and Cs atomic vapors [1-3].

For the EIT-resonance successful formation the following new rule has been established: if one of the transitions of the Λ - system is formed by a magnetically induced atomic transition for which the condition $F_e - F_g = \Delta F = +2$ is satisfied, then both the probe and the coupling radiation must have σ^+ polarization. Meanwhile, if one of the transitions of the Λ - system is formed by a magnetically induced atomic transition for which the condition $F_e - F_g = \Delta F = -2$ is satisfied, and then both the probe and the coupling radiation must have σ^- polarization.

Thus, the generation of EIT resonances is affected by the circular dichroism induced by the presence of a magnetic field [4].

This work was supported by the State Committee for Science, Ministry of Education and Science of the Republic of Armenia (project no. N21T-1C005).

References

- [1] A. Sargsyan, A. Tonoyan, A. Papoyan, D. Sarkisyan, *Opt. Lett.* **44**, 1391 (2019).
- [2] A. Sargsyan, T. A. Vartanyan, D. Sarkisyan, *Opt. and Spectr.*, **128**,12 (2020).
- [3] A. Sargsyan, A. Tonoyan, D. Sarkisyan, *JETP*, **133**,16 (2021)
- [4] A. Sargsyan, A. Amiryan, A. Tonoyan, et al., *Physics Lett. A* **434**, 128043 (2022).

Spectral and Tuning Characteristics of Extended Cavity Diode Lasers

A. P. Bogatov¹, A. E. Drakin¹, D. S. Chuchelov¹, E. A. Tsygankov¹, V. V. Vassiliev¹,
M. I. Vaskovskaya¹, V. L. Velichansky^{1,2}, S. A. Zibrov¹

¹ *P. N. Lebedev Physical Institute, Russian Academy of Sciences, 119991 Moscow, Russia*

² *National Research Nuclear University MEPhI (Moscow Engineering Physics Institute), 115409
Moscow, Russia.*

Email: vlvlab@yandex.ru

It is easy to tune the wavelength of an edge-emitting diode laser (DL) by a control of its current and/or temperature. The drawbacks of this technique are relatively large linewidth and mode hopping. Both problems are solved in extended cavity diode lasers (ECDL). That is why they are widely used in high-resolution spectroscopy, cooling of atoms, metrology and quantum optics. Here, we focus on distinctive features of ECDL as compared with other types of tunable lasers. Usually, a selective element is inserted into a laser cavity to tune the wavelength within a large part of a gain width. It is similar to other types of tunable lasers. What is different, however, is that the own cavity of a DL serves as an additional selective element whose frequency and width depend on the gain, which is equal to the total loss of the cavity. It stems from a residual reflection from a facet of a DL chip. Another reason is nonlinearity of the refractive index. The saturated gain and electron concentration in active region of a laser depend on field intensity (and losses of the cavity) while refractive index depends on electron concentration. We demonstrate that the quasi-stationary wavelength tuning is influenced by a strong interconnection of ECDL parameters resulting in tuning hysteresis and cusp-like change of laser power during a mode hopping.

Similar interconnection reveals itself in fast dynamics of a single mode laser. It results in self-stabilization of a single mode operation, noise suppression, and dynamic splitting of longitudinal modes. We describe the last feature in some detail. We disclose it in the frequency dependence of the modulation efficiency of an ECDL [1]. Its FM response to the microwave current modulation has two maxima whose frequencies are close to the frequency difference of the adjacent longitudinal modes. The splitting depends on the power of laser radiation. We have observed similar splitting in AM noise spectra with the same type of dependence on power. The peculiarity of the AM noise spectrum was observed and explained by the nonlinear interaction of fields in the active region of a DL [2]. The dynamic splitting of the laser cavity modes explains the specific features of the modulation characteristics.

We discuss also problems of DL multimode operation, phase noise suppression, and possible way to increase power of highly coherent laser radiation.

References

- [1] S.A. Zibrov, D.S. Chuchelov, A.E. Drakin, *et al.*, *IEEE J. Quantum Electron.*, **56**(3), 2000607 (2020).
- [2] A. Bogatov, P. Eliseev, O. Kobildzhanov, *et al.*, *IEEE J. Quantum Electron.*, vol. **QE-23**, 1064 (1987).

Femtosecond Lasers in Ophthalmology: Finite Element Modeling of Glaucoma Surgery

G. P. Djotyan^{1,2}, E. R. Mikula^{2,3}, K. Kranitz⁴, Z. Nagy⁴, T. Juhasz^{2,3}

¹*Wigner Res. Centre for Phys., Budapest, Hungary*

²*Dep. of Ophthalmol., Univ. of California, Irvine, Irvine, CA, USA*

³*ViaLase Inc., Aliso Viejo, CA, USA*

⁴*Dep. of Ophthalmol., Semmelweis Univer., Budapest, Hungary*

Email: dzsotjan.gagik@wigner.hu

Femtosecond laser pulses can achieve laser induced optical breakdown at relatively low pulse energies and can be safely delivered to different parts of eye by selecting the proper wavelength and scanning patterns. In this talk, we concentrate on application of femtosecond laser radiation in glaucoma surgery, namely on the femtosecond laser trabeculotomy (FLT) treatment [1]. Glaucoma is a disease accompanied by increasing of the intraocular pressure (IOP) in eye resulting in damage to the optical nerve, leading to vision loss. Elevated IOP is primarily due to an increase of resistance to outflow of aqueous humor (AH) of some elements of drainage system of eye. Current glaucoma treatments include drug and surgical treatments to both decrease AH formation and to increase AH outflow facility. Surgical treatments offer potential advantages over drug therapies. Among the surgical treatments, the FLT seems to be one of the most perspective one due to its minimally invasive nature and relatively large value of achieved IOP reduction along with excellent safety profile.

We present the results of finite element modeling (FEM) of FLT [2] that show high potential in prediction of the results, as well as in optimization of the FLT treatment. The FEM simulations are performed using Comsol Multiphysics software. Navier–Stokes and Darcy’s equations are numerically solved for AH flow in the drainage system of eye.

References

[1] E.R. Mikula, F. Raksi, I.I.Ahmed et al. *Translat. Vis. Sci. & Techol.*, **11**, 28 (2022).

[2] E.R. Mikula, G.P. Djotyan, K. Kranitz, et al., *Invest. Ophthalmol. Vis. Sci.* **63**, 166 (2022).

Bessel Beam Assisted Photovoltaic Trapping of Micro/nano-objects on a Lithium Niobate Crystal

L. Tsarukyan¹, A. Badalyan¹, L. Aloyan², Y. Dalyan², R. Drampyan¹

¹*Institute for Physical Research, National Academy of Sciences of Armenia, Ashtarak-2, 0204, Armenia*

²*Yerevan State University, 1 Alek Manukyan st., 0025, Yerevan, Armenia*

Email: rafael.drampyan@gmail.com

We report on the design and fabrication of chip-scale and high-performance photovoltaic tweezers based on photorefractive lithium niobate (LN) crystal and nondiffracting Bessel beam technique. The novelty of our approach is the combination of unique features of non-diffracting optical beams and perfect photorefractive and electro-optical properties of lithium niobate crystals for the elaboration of photovoltaic tweezers.

The Bessel beam provides the formation of high-contrast and large modulation depths, micrometric-scale, 2D photovoltaic fields ($\sim 10^7$ V/m) distribution in the LN crystal volume and *near its surface*. The generated strong electric fields act on micro/nano-objects via dielectrophoretic (DEP) forces providing their 2D trapping and manipulation on the crystal surface. The advantage of properly doped LN crystals is that photovoltaic fields remain for a very long time (a few months) in the crystal thanks to its high resistance thus providing the operation of *chip-scale* photovoltaic tweezers in an autonomous regime.

For the experimental realization of photovoltaic tweezers, the Fe-doped LN crystal was illuminated by a 40 mW power Bessel beam at 532 nm wavelength that induces the refractive Bessel lattice with $40\mu\text{m}$ periodicity inside the crystal and a corresponding photovoltaic field distribution on the crystal surface [1]. The photovoltaic tweezers were applied to trapping and manipulation of dielectric CaCO_3 microparticles, Ag nanoparticles in glycerin suspension and DNA molecules dissolved in NaCl buffer. Fig. 1(a) shows the phase microscope image of the trapping of DNA on the LN:Fe crystal surface. According to the Bessel beam-induced photovoltaic fields and DEP forces map, DNA molecules are localized at the borderlines of the Bessel rings, clearly seen in the enlarged pattern in Fig. 1(b).

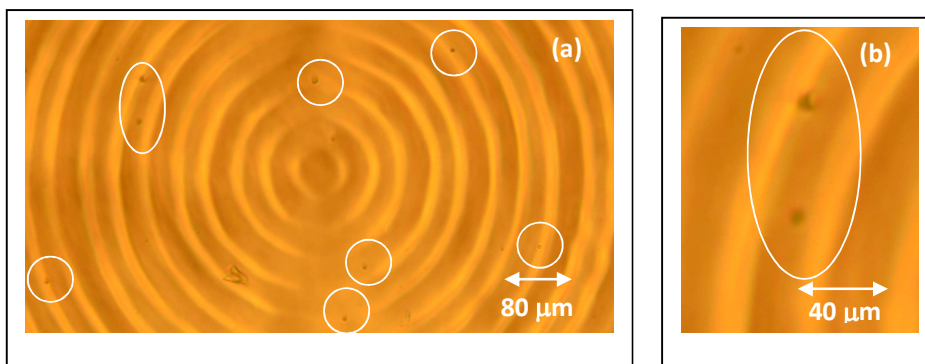


Fig. 1

Particle manipulation techniques are of crucial importance in many fields of research, from integrated optics and photonic devices to micro/nanoelectronics and biotechnology.

References:

[1] L. Tsarukyan, A. Badalyan, R. Hovsepyan, R. Drampyan, *Opt. Las. Techn.* **139**, 106949 (2021).

Invited report

Magneto Plasmon Spectrum in Graphene

A. M. Ishkhanyan^{1,2}, V. P. Krainov³

¹*Russian-Armenian University, 0051 Erevan, Armenia*

²*Institute for Physical Research of NAN Armenia, 0203 Ashtarak, Armenia*

³*Moscow Institute of Physics and Technology (National Research University), 141070 Dolgoprudny, Russia*

Email: vpkrainov@gmail.com

Due to their promising properties, surface magneto plasmons have attracted great interest in the field of plasmonics. 2D material-graphene shows great potential in infrared magnetic plasmonics [1-5]. Anomalous dependence of the plasmon spectrum on the external magnetic field was reported in [2-3]. We consider analytically propagation of longitudinal surface plasma waves in graphene in the presence of external magnetic field using the kinetic Boltzmann equation. The linear Dirac spectrum of the electrons in graphene is $\varepsilon = \pm v|\mathbf{p}|$. It was shown that the role of the magnetic field is important at small plasmon frequencies. The dependence of the square of the frequency on the wave number k in the case of the arbitrary magnetic field is of the form

$$\omega^2 = \frac{1}{2}\kappa k + \omega_c^2 + \frac{1}{2}\kappa k \sqrt{1 + \frac{8\omega_c^2}{\kappa k}}. \quad (1)$$

Here $\kappa = \frac{2e^2\varepsilon_F}{\hbar^2\varepsilon_s}$, ε_s is dielectric constant, $\omega_c = \frac{ev^2B}{c\varepsilon_F}$, B is the magnetic field strength. It follows from Eq. (1) at the weak magnetic field B , the known dependence of the perturbation theory [4]:

$$\omega^2 = \kappa k + 3\omega_c^2. \quad (2)$$

References

[1] Bin Hu, Surface magneto plasmons and their applications, in “Plasmonics”, ed. by Tatjana Gric, IntechOpen, (2018).

[2] Bin Hu, J. Tao, Y. Zhang, and Q. Wang, *Optics Express*, **22**, 21727 (2014).

[3] M. Heydari and M. Samiei, Magneto-Plasmons in Grounded Graphene-Based Structures with Anisotropic Cover and Substrate, <https://arxiv.org/abs/2103.08557> (2021).

[4] M. O. Goerbig, *Rev. Mod. Phys.* **83**, 1193 (2011).

[5] J.Guo, X. Dai, Y. Xiang and D. Tang, Journal of Applied Physics, **125**, 013102 (2019).

Invited report

MacColl-Hartman Paradox Interpretation: a Challenge to the Wave Equation

A. Zh. Muradyan

Institute of Physics, Yerevan State University, 0025, 1 Alex Manoogian, Yerevan, Armenia

Email: muradyan@ysu.am

The phase velocity of a stationary state is twice the classical propagation velocity. To overcome this issue, the stationary state is replaced by a wave packet, whose group velocity reproduces the classical velocity. Based on this approach, MacColl semi-quantitatively considered the problem of the time of sub-barrier tunneling and came to the intriguing conclusion that "there is no appreciable delay in the transmission of the packet through the barrier" [1]. This issue has not been touched upon for a long time, perhaps because it was not possible to approach it experimentally. During the advent of semiconductor technologies, Hartman reconsidered the problem [2] and concretized the essence that the sub-barrier tunneling time is saturated versus the width of the potential barrier. This paradoxical conclusion contradicts the special theory of relativity limiting the velocities to the speed of light. Extensive list of articles concerning the problem (e.g. see in [3]) explains the complexity of situation, but don't answer the question why the sub-barrier tunneling time slows down versus the width of the barrier and for wide barriers ceases to grow at all (Fig. 1).

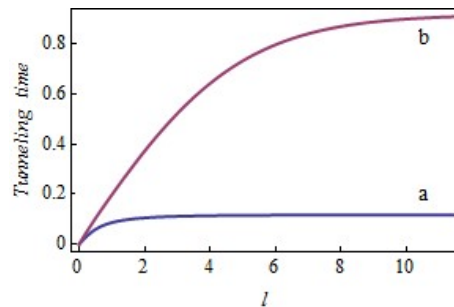


Fig. 1. (a) Phase and (b) group time of sub-barrier tunneling versus the barrier width.

This report is just presents the “counterintuitive” mathematical structure of the formation of this paradox [4]. It is also shown that the mechanism of formation of the propagation time is not the priority of sub-barrier tunneling only, but it continues (albeit with a gradual weakening) also into the over-barrier region. This is inextricably linked with the propagation of any wave packet in a potential field and thereby creates a principal problem for the wave equation and needs a thorough experimental verification.

References

[1] L.A. MacColl. Phys. Rev. vol.40, p. 621-626, 1932.

- [2] T.E Hartman. J. Appl. Phys. Vol. 33, p. 3427-3433, 1962.
[3] R. Ramos, D. Spierings, I. Racicot and A.M. Steinberg, Nature, vol. 583, p. 529-532, 2020.
[4] A.Zh. Muradyan, arXiv: quant-ph/2108.03054, 2021.

Invited report

Atomic Limit in Optical Microscopy & Photon Confinement: Tip-Enhanced Raman Scattering in the Atomistic Near-field

V. A. Apkarian

Department of Chemistry, University of California at Irvine, Irvine CA 92697, USA

Email: aapkaria@uci.edu

To the extent that we see objects by the light they scatter, it is now possible to see atoms, albeit using a plasmonic lens to focus light down to the size of an atom. We have illustrated this through the first ever atom-resolved optical images of surfaces [1], electric currents and mechanical vibrations (phonons) inside a single molecule [2]. This natural limit in resolution, which is ultimately determined by the atomic granularity of matter, is attained through tip-enhanced Raman spectro-microscopy (TERS) in the atomistic near-field (ANF). We use an atomically sharp silver needle to couple light into the subatomic junction gap of an ultra-high vacuum cryogenic scanning tunneling microscope (STM) [3]. The implemented superfocusing of light was predicted by the seminal works of Nerkararyan and coworkers, who pointed out that unlike diffractive optics, classically, there is no limit to confinement of light guided by a tapered plasmonic nanowire [4,5]. In practice, the classical singularity is eliminated by the quantization of matter (its atomic granularity), which determines the natural limit in image resolution. We show that the same limit holds for confinement of the photon: the apex mode of an atomically terminated needle is confined to the terminal atom. In effect, the waveguided photon adiabatically converts to matter by acquiring mass and charge. In this limit, optics and electronics merge, photons can be directly wired into molecular electronic circuitry, and entangled light-matter states generalize as quantization of the dielectric. Quantum plasmonics in the ANF gives simultaneous access to pico-photonics and pico-electronics, it opens up the post-nano era of picoscience, which we demonstrate through illustrative examples.

References

- [1] K. T. Crampton, J. Lee, V. A. Apkarian, ACS Nano **13**, 6363 (2019).
[2] J. Lee, K. T. Crampton, N. Tallarida, V. A. Apkarian, Nature **568**, 7750 (2019).
[3] N. Tallarida, J. Lee, V. A. Apkarian, ACS Nano **11**, 11393 (2017).
[4] Kh. V. Nerkararyan, Phys. Lett. A. **237**, 103 (1997)
[5] A. J. Babadjanyan, N. L. Margaryan, Kh. V. Nerkararyan, J. Appl. Phys. **87**, 3785 (2000).

Preparation and Study of Graphene/LN Heterojunction for Sensorial Application

E. Kokanyan^{1,2}, N. Margaryan³, N. Gasparyan³, N. Babajanyan¹

¹Armenian State Pedagogical University after Kh.Abovyan, Yerevan, Armenia

²Institute for Physical Research, National Academy of Sciences of Armenia, Ashtarak Armenia

³A. Alikhanyan National Science Laboratory (Yerevan Physics Institute), Yerevan, Armenia

Email: edvardkokanyan@gmail.com

Due to their outstanding physical properties, graphene and related materials have a huge potential for applications in electronic and optical devices. In our research graphene layers are obtained by liquid phase exfoliation (LPE) method for the application in SAW sensors. On the other hand, stoichiometric lithium niobate (LN) is the best material for such applications, because of its piezoelectric character and unique physical characteristics.

Synthesized in a colloidal solution, graphene layers are substituted to LN substrate and studied. As the fingerprint of graphene and other carbon nanomaterials, the spectrum of Raman scattering is measured and analyzed (Fig. 1).

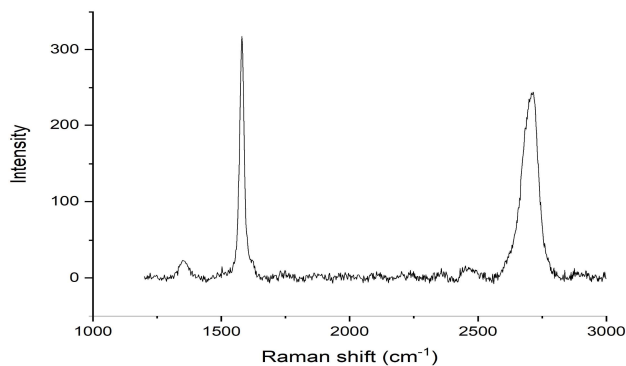


Fig. 1. Raman spectrum of the layer graphene deposited on LN

The current- voltage characteristics of graphene deposited on LN are measured and studied using data acquisition devices and LabVIEW programming. The studies revile the influence of screening effect on the electrical properties of graphene, because of high dielectric constant of LN crystal.

Electromagnetically Induced Absorption Resonances in Alkali-Metal Vapor Cells for Applications in Quantum Metrology

D. V. Brazhnikov^{1,2}, V. I. Vishnyakov¹, S. M. Ignatovich¹, M. N. Skvortsov¹

¹ *Institute of Laser Physics SB RAS, 15B Lavrentyev Ave, Novosibirsk 630090, Russia*

² *Novosibirsk State University, 1 Pirogov Str, Novosibirsk 630090, Russia*

Email: brazhnikov@laser.nsc.ru

The coherent population trapping (CPT) is one of the brightest representatives of the nonlinear optical effects caused by interference of dipole transitions in atoms. It is often observed as a “dark” resonance in the intensity of light beam transmitted through a vapor cell. One of the main features of this resonance is that it can have a very narrow (subnatural) linewidth. CPT resonances have been successfully applied to the development of miniature atomic clocks. Another example of the nonlinear interference effects is electromagnetically induced absorption (EIA) that is usually observed as a “bright” subnatural-width resonance. At the contrary of the CPT resonances, the exploitation of the EIA ones has been rarely explored for the development of atomic clocks. Here, we study a pump-probe scheme that exhibits two-frequency EIA resonances in a 5-mm length Cs vapor cell and can be used for the development of microwave frequency standards. The short-term frequency stability is presented in Fig.1a.

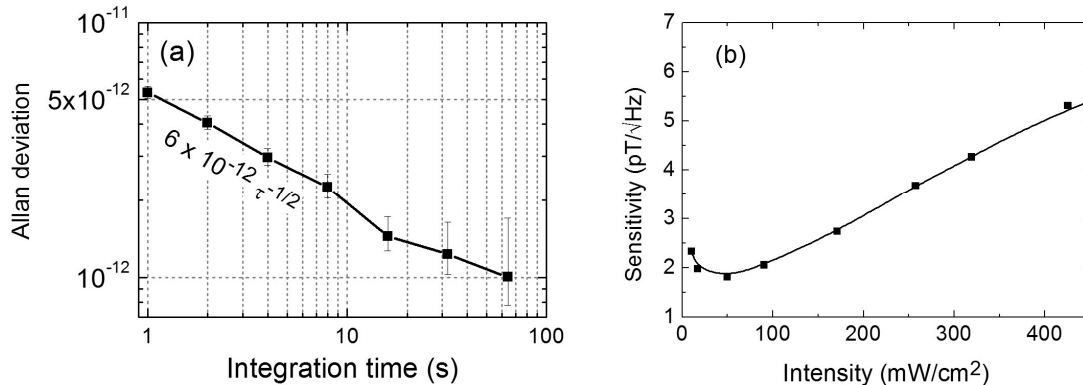


Fig. 1. (a) Stability of the EIA-based frequency standard, (b) Magnetic-field sensitivity.

The ground-state Hanle effect (GSHE) is also a nonlinear interference effect. It underlies the most robust and simple techniques in quantum magnetometry. In the miniature GSHE-sensors, a single circularly polarized light wave and a transverse magnetic field are used to observe the electromagnetically induced transparency (EIT) resonance. To increase a contrast-to-width ratio (CWR), GSHE-sensors require a relatively high temperature of vapors (up to 180°C) that undesirable for some applications. Here, we study several new schemes that can be used for increasing CWR at relatively low temperatures. In particular, we use a single elliptically polarized wave and a polarimetric technique to observe the EIA resonance at 60°C in Cs vapors. Using a small cell ($\ll 1 \text{ cm}^3$), our setup exhibits a sensitivity of $1.8 \text{ pT}/\sqrt{\text{Hz}}$ (Fig.1b). We thank RSF (22-12-00279) and RFBR (20-02-00075).

Simulation of Terahertz Radiation Generation by Femtosecond Pulses Propagating in Nanocomposites with Semiconductor Quantum Dots

O. Fedotova¹, A. Husakou², R. Rusetski¹, O. Khasanov¹, A. Fedotov³, T. Smirnova⁴, U. Sapaev⁵, P. Klenovsky^{6,7}, and I. Babushkin^{8,9,2}

¹*SPMRC of NASB, P. Brouki 19, Minsk 220072, Belarus*

²*Max Born Institute, Max Born Str. 2a, 12489 Berlin, Germany*

³*Belarusian State University, Nezalezhnasci Ave. 2, Minsk 220030, Belarus*

⁴*ISEI BSU, Dauhabrodskaya str. 23, Minsk, Belarus*

⁵*TSTU, st. University 2, Olmazar district, 100095 Tashkent, Uzbekistan*

⁶*Masaryk University, Kotlářská 267/2, 61137 Brno, Czech Republic*

⁷*Czech Metrology Institute, Okružní 31, 63800 Brno, Czech Republic*

⁸*IQO, Leibnitz Hannover University, Welfengarten 1, 30167 Hannover, Germany*

⁹*Cluster of Excellence PhoenixD, Welfengarten 1, 30167 Hannover, Germany*

Email: ewynknight@gmail.com

Large values of permanent dipole moment (PDM) are revealed ($10^2 - 10^3$ Debye) in nanostructures like semiconductor quantum dots (QDs) of ZnO, ZnS, CdSe what is comparable with values of transition dipole moments between the exciton states. As well, the additional transitions between exciton states allowed due to PDM may play a significant role in the nanoparticle response, in particular for the generation of new frequencies in the of terahertz (THz) range [1]. We study THz generation in in nanocomposites consisted of QD inclusions (ZnO) in transparent dielectric matrix (SiO₂ host). Pumping pulse carrier frequency is supposed to be in resonance with the frequency transition between lower excitonic states. Theoretical models allowing study coupled resonant and non-resonant mechanisms of frequency down and up conversion in nanocomposite have been developed. Simulations of the pulse propagation were performed on the base of self-consisted system for the density matrix (Bloch) equations describing multilevel excitonic transitions and the unidirectional propagation equation, accounting for chromatic dispersion, second- and third-order optical nonlinearities of both host and inclusions, photoionization of inclusions, plasma dynamics (in case of higher pulse input power) and its influence on the dielectric function of the inclusions. As an analysis shows, for the case of PDM smaller than 10 Debye and moderate input intensity (less than 0.07 TW/cm²) the output efficiency of THz may reach 0.23% after 50 mkm of propagation of two 15-fs pulses at central circular frequencies (FWHM) of 2.26 fs⁻¹ and 2.40 fs⁻¹, what may be explained by significant exciton resonance contribution. With increase of the input intensity up to 1 TW/cm² and PDM up to 100 Debye for pulse propagating over distances 50 mkm in nanocomposite it is established that the THz part of the spectrum is increased with the propagation distance. The THz efficiency at the same propagation length is by 2-3 order of magnitude more for the case with lagrer PDM. The few approaches to the real level structure computation have been proposed.

Reference

[1] S. B. Bodrov, A. N. Stepanov, and M. I. Bakunov, *Opt. Express* 27, 2396 (2019).

Versatile Tools for Manipulating Light Enabled by the 4th Generation Optics

N. Tabiryan

BEAM Engineering for Advanced Measurements Co., Orlando, Florida, USA

Email: nelson@beamco.com

The purpose of the presentation is to introduce the new generation planar optics science and technology and its advantages compared to metalens and other planar optics technologies. Indeed, manufacturing difficulties set practical limitations for fabrication and performance of metamaterial based optics for visible and shorter wavelengths. Optimization and fabrication of metalenses of macroscopic sizes is particularly a challenge. These limitations are fully overcome by diffractive waveplate technology [1,2]. Planar lenses of near 100% efficiency even for UV wavelengths have been demonstrated using liquid crystal polymers. We have also demonstrated planar optical components with unprecedentedly broad bandwidths of near 100% efficiency for visible as well as infrared wavelength. Spectral engineering inherently feasible for diffractive waveplate technology allows versatile customization of diffraction efficiency spectra.



Fig. 1. The first known lens, the 3000 year old Nimrud lens, exhibited at British Museum, shown with the last, the 4th generation lens made at BEAM Co.

The technology has numerous applications for all modern and future applications, spanning from adaptive ophthalmic lenses to solar sails [3].

References

- [1] N.V. Tabiryan, D.E. Roberts, D.M. Steeves, and B. Kimball, *Photonics Spectra*, March, **46** (2017).
- [2] N.V. Tabiryan, D.E. Roberts, Z. Liao, *et al.*, *Adv. Optical Mater.*, 2001692 (2021).A.
- [3] A.R. Davoyan, J.N. Munday, N.V. Tabiryan, *et al.*, *Optica* **8**, 722 (2021).

Abstracts of Oral Reports

Simulating Universal Gaussian Circuits with Linear Optics

L. Chakhmakhchyan^{1,2}, N. J. Cerf¹

¹ Centre for Quantum Information and Communication, Ecole polytechnique de Bruxelles, CP 165,
Université libre de Bruxelles, 1050 Brussels, Belgium

² Krisp, Hrachya Kochar 5/1, Yerevan 0033, Armenian

Email: levon.chakhmakhchyan@gmail.com

Recent advances in the theory and technology of quantum photonics have established it as one of the most promising candidate platforms to realize operational quantum technologies [1]. A wave of remarkable progress in quantum photonics has come, in part, after Aaronson and Arkhipov proved that highly demanding measurement-induced circuit control is not necessary to outperform a classical computer [2]. Despite being of fundamental importance, however, such a *linear* computational setting suffers from several drawbacks, as e.g., a lack of practical applications and the necessity of a high number of photons for achieving a quantum advantage (~50 photons distributed among ~2500 modes).

A possible strategy to overcome this situation is to develop specialized sub-universal photonic setups, which lie in-between linear optics and universal quantum computation. That is, identify a class of photonic circuits augmented with post-processing so to implement a restricted but exploitable set of non-linearities. We adopt this very approach and develop a scheme enabling us to simulate sampling from an arbitrary *Gaussian* circuit.

Our method for simulating Gaussian circuits relies on the Bloch-Messiah decomposition but introduces a major improvement. This decomposition implies that an arbitrary Gaussian transformation can always be mapped onto two linear-optical circuits intermitted by a layer of single-mode squeezers, hence requiring non-linear optical media. In contrast, our approach circumvents the need for in-line nonlinearity and requires two-mode squeezed vacuum states as a prior resource only. The building block of our procedure lies in that a two-mode squeezer is equivalent to a beam splitter undergoing partial time reversal, allowing the conversion between passive and active optics [3].

In fact, current and emerging integrated photonic technologies, such as silicon-based photonic hardware, make a good candidate platform for the realization of our scheme. The on-chip nonlinearities enable one to generate resource two-mode squeezed vacuum states via degenerate spontaneous four-wave mixing. The state evolution and detection can, in turn, be implemented by means of manufacturable programmable photonic circuitry (with ≈ 0.2 dB loss per beam splitter transformations) and (integrated) superconducting photo-detectors (reaching 70-80% efficiencies) [6].

References

- [1] F. Flamini, N. Spagnolo, F. Sciarrino, *Rep. Prog. Phys.* **82**, 016001 (2018).
- [2] S. Aaronson, A. Arkhipov, *Theory of Computing* **9**, 143 (2013).
- [3] L. Chakhmakhchyan, N. J. Cerf, *Phys. Rev. A* **98**, 062314 (2019).
- [5] J. Wang, S. Paesani, et al., *Science* **360**, 285 (2018).

Shallow Donors in Gapped Graphene Systems

A. P. Djotyan, A. A. Avetisyan

Department of Physics, Yerevan State University, Yerevan, 0025, 1 A. Manoogian

Email: adjotyan@ysu.am

Single layer graphene (SLG), a two-dimensional form of carbon, attracted a great theoretical and experimental interest due to Dirac-type spectrum of charge carriers in this gapless semiconductor. The discovery of graphene brought an exciting link between solid-state physics and quantum electrodynamics (QED). Due to zero band gap, graphene monolayer cannot be applied in on–off devices. To apply graphene in such devices, it is necessary create a band gap between valence and conduction bands in graphene.

The interest on graphene systems with opened energy gap derives from its great potential for applications in nano- and optoelectronics, e.g. for creation of new spintronic devices, novel lasers and quantum information processing.

More intriguing system is bilayer graphene (BLG) which consists of two coupled graphene layers. One of the preferences of BLG is its tunable band gap which can be opened by applying a perpendicular electric field and continuously tuned from a few to nearly 300 meV [1, 2].

The development of graphene-based devices requires a better understanding the physics of isolated impurity state in doped graphene systems with opened energy gap, where the binding energy of impurity electron and its localization length depend on the concentration of charge carriers, the band gap value, tight binding parameters, and can be controlled by application of external electric and magnetic fields. For fundamental physics as well as for different applications it is interesting to develop transparent analytical methods for solving the Coulomb problem in BLG with its complicated dispersion law.

In this work, using developed variational approach, we calculated the ground state energy of an isolated impurity electron in doped SLG and BLG with opened energy gap in a perpendicular magnetic field taking into account the screening of Coulomb interaction [3,4].

The dependencies of the ground state binding energy and localization length of an impurity electron on the gap value, dielectric constant, strength of the magnetic field, the dopants concentration and tight binding parameters are obtained.

References

- [1] E. V. Castro, K. S. Novoselov *et al*, *Phys. Rev. Lett.* **99**, 216802 (2007).
- [2] A. A. Avetisyan, B. Partoens, and F. M. Peeters, *Phys. Rev. B* **81**, 115432 (2010).
- [3] E. H. Hwang and S. Das Sarma, *Phys. Rev. Lett.* **101**, 156802 (2008).
- [4] P. K. Pyatkovskiy, *Journal of Physics: Condensed Matter* **21**, 025506 (2008).

Oral report

On the Method and Results of Calculation of the Tetrahedral Splittings and Resonance Interactions in Vibrational Spectra of High Symmetry Molecules

E. S. Bekhtereva, O. N. Ulenikov, O. V. Gromova, N. I. Nikolaeva

Research School of High-Energy Physics, National Research Tomsk Polytechnic University, Lenin av., 30, 634050, Tomsk, Russia

Email: bextereva@tpu.ru

We report here the general analytical description of one of the most difficult problems in the study of high symmetry quantum mechanical objects, namely, of tetrahedral splittings caused by the high symmetry of a molecular object. On the basis of the derived general results, vibrational tetrahedral splittings are presented in analytical form and applied for the description of the vibrational energy spectrum of the CH₄ molecule as example of XY₄ molecules with T_d symmetry.

This research was supported by TPU development program Priority 2030 (project NIP/EB-010-0000-2022).

Oral report

Generation of Two Entangled Photons During the Decay of a Single Photon in an Optical Fiber with Random Boundaries

A. S. Gevorkyan^{1,2}

¹*Institute for Informatics and Automation Problems, NAS of RA*

²*Institute of Chemical Physics, NAS of RA*

Email: g_ashot@sci.am

Abstract. Entanglement of the spatial degrees of freedom of photons is one of the most important directions for the implementation of quantum communications. There are various rather complex and expensive experiments on the generation of entangled photons, in which the environmental noise is the main factor in the decoherence of these states. Optical waveguides are often used to transport spatially entangled photons because such systems are capable of supporting multiple transverse modes. We are studying the possibility of generating entangled photons from single photons directly in the light guide. In particular, the problem is considered when the boundaries of the fibers are scabrous, so that during the propagation of single circularly polarized photons, an external force consisting of regular and random components acts on them. Mathematically, the problem is formulated as a quantum equation for a single photon in an arbitrary medium, including those with random properties. In particular, using the obvious similarity between a neutrino and a photon, we

proved that the propagation of a photon in a 3D inhomogeneous medium can be described by an equation of the Lagevin-Weyl type:

$$\partial_t \Psi_{\pm}(\mathbf{r}, t) \pm c(\mathbf{r})(\mathbf{S} \cdot \nabla) \Psi_{\pm}(\mathbf{r}, t) = 0, \quad \partial_t = \partial / \partial t, \quad (1)$$

where $c(\mathbf{r})$ denotes the speed of light in the medium, $\Psi_{+}(\mathbf{r}, t)$ and $\Psi_{-}(\mathbf{r}, t)$ are photons of both helicities, a left-hand +1 and right-hand -1, correspondingly. In (1) $\mathbf{S} = (S_x, S_y, S_z)$ is a set of matrices, where each of them has the form:

$$S_x = \begin{pmatrix} 0 & 0 & 0 \\ 0 & 0 & -i \\ 0 & i & 0 \end{pmatrix}, \quad S_y = \begin{pmatrix} 0 & 0 & i \\ 0 & 0 & 0 \\ -i & 0 & 0 \end{pmatrix}, \quad S_z = \begin{pmatrix} 0 & -i & 0 \\ i & 0 & 0 \\ 0 & 0 & 0 \end{pmatrix},$$

in addition, $\nabla = (\partial/\partial x, \partial/\partial y, \partial/\partial z)$ is a Nabla operator and $\mathbf{r} = (x, y, z)$ is the photon radius vector. From the first order equation (1), we can find the following second-order partial differential equation (PDE):

$$\partial_t^2 \Psi_{\pm}(\mathbf{r}, t) - c(\mathbf{r})(\nabla c(\mathbf{r}) \nabla) \Psi_{\pm}(\mathbf{r}, t) + c^2(\mathbf{r}) \nabla \cdot (\nabla \Psi_{\pm}(\mathbf{r}, t)) = 0. \quad (2)$$

Finally, substituting the solution of equation (2) in the form:

$$\Psi_{\pm}(\mathbf{r}, t) \approx \exp(i\omega_0 t + ik_z z) F_{\pm}^{\eta}(x, y, 0), \quad \eta = (x, y),$$

for the propagation of the wave function component, we get the following parabolic PDE:

$$\left\{ i \frac{\partial}{\partial \tau} + \frac{1}{2} \left(\frac{\partial^2}{\partial x^2} + \frac{\partial^2}{\partial y^2} \right) + \frac{c_{;x}(y)}{2c} \frac{\partial}{\partial x} + \left(\frac{\omega_0^2}{c^2} - k_z^2 \right) \right\} F_{\pm}^{x(y)}(\mathbf{r}, t) = 0, \quad \tau = \frac{z}{k_z}, \quad (3)$$

where ω and k_z denote the frequency and momentum of the photon. Finally expanding the speed of light near the z-axis, from (3) we can find the following stochastic equation:

$$\left\{ i \frac{\partial}{\partial \tau} + \frac{1}{2} \left(\frac{\partial^2}{\partial x^2} + \frac{\partial^2}{\partial y^2} \right) - \frac{1}{2} \left(A_1(\tau)x^2 + A_2(\tau)y^2 + A_0(\tau)xy \right) \right\} F_{\pm}^x(\mathbf{r}, t) = 0, \quad (4)$$

where $A_0(\tau) = \frac{\omega_0^2}{c_0^2} c_{xy}(0, 0, z)$, $A_1(\tau) = \frac{\omega_0^2}{c_0^2} c_{xx}(0, 0, z)$ and $A_2(\tau) = \frac{\omega_0^2}{c_0^2} c_{yy}(0, 0, z)$, in

addition, $c_{xy}(0, 0, z) = \partial_{xy}^2 c(\mathbf{r})|_{x=y=0}$. In the case when $c_{xx}(0, 0, z) = c_{yy}(0, 0, z) > 0$, equation (4) describes the motion of a single photon with circular polarization. If randomness is defined as a Gauss-Markov process, then, as shown in [1], it is possible to construct all the statistical parameters of

a photonic system in the form of multiple integrals and solutions of reference partial differential equations.

In this paper, formulas are obtained for the probability of decay of single photons into two entangled photons. A mathematical apparatus has been developed for studying the possibilities of controlling the parameters of entangled photons using the characteristic features of random processes.

- [1] A.S. Gevorkyan et al, Hidden Dynamical Symmetry and Quantum Thermodynamics from the First Principles: Quantized Small Environment, *Symmetry* 2021, **13**, 1546. <https://doi.org/10.3390/sym13081546>

Oral report

High Resolution Ro–Vibrational Analysis of Molecules in Doublet Electronic States: the $\nu_1+\nu_3$ Band of Chlorine Dioxide ($^{16}\text{O}^{35}\text{Cl}^{16}\text{O}$) in the X^2B_1 Electronic Ground State

O. N. Ulenikov¹, E. S. Bekhtereva¹, O. V. Gromova¹, S. Bauerecker²

¹ *Research School of High-Energy Physics, National Research Tomsk Polytechnic University, Lenin av., 30, 634050, Tomsk, Russia*

² *Institut für Physikalische und Theoretische Chemie, Technische Universität Braunschweig, D-38106, Braunschweig, Germany*

Email: ulenikov@mail.ru

We report the spectrum of the $\nu_1+\nu_3$ band of chlorine dioxide measured with essentially Doppler limited resolution at an instrumental line width of 0.001 cm^{-1} using the Zurich prototype ZP2001 Bruker IFS 125 HR Fourier transform infrared spectrometer. The ro–vibrational line analysis is carried out with an improved effective Hamiltonian and a newly developed computer code ROVDES for the ro–vibrational spectra of open-shell free radical molecules including spin–rotation interactions. Accurate values of rotational, centrifugal and spin–rotational parameters were determined for $^{16}\text{O}^{35}\text{Cl}^{16}\text{O}$ in the vibronic ground state X^2B_1 from more than 3500 ground state combination differences. The 7239 assigned transitions for the $\nu_1+\nu_3$ band with $N^{\text{max}} = 76$ and $K_a^{\text{max}} = 26$ provide a set of 32 accurate effective Hamiltonian parameters for the $\nu_1+\nu_3$ band ($(\nu_1 \nu_2 \nu_3) = (101)$ (21 rotational and centrifugal distortion parameters and 11 spin–rotational interaction parameters). This effective Hamiltonian (A–reduction and I^r–representation) reproduces 1703 upper state energies from the experiment with a root-mean-square deviation $d_{\text{ms}} = 1.67 \times 10^{-4}\text{ cm}^{-1}$ and the 7239 transition wavenumbers with $d_{\text{ms}} = 3.45 \times 10^{-4}\text{ cm}^{-1}$. Our results provide a considerable improvement over previous results with which we compare and should provide a benchmark for theoretical studies with applications to atmospheric spectroscopy and laser chemistry.

The research was funded by the Russian Science Foundation, project 22-22-00171.

Oral report

Atom-Surface Interaction in a Potassium Nanocell

A. Sargsyan, D. Sarkisyan

Institute for Physical Research, National Academy of Sciences of Armenia, Ashtarak, 0203 Armenia

Email: sargsyanarmen85@gmail.com

The effect of the dielectric surface on the atomic transitions of ^{39}K D_1 line at nanometer distances has been experimentally studied [1]. A nanocell which filled with atomic potassium and has a wedge gap has been used to study the interaction of atoms at distances of 50–800 nm with the technical sapphire window surface. At distances $L < 100$ nm from the sapphire surface, the van der Waals interaction strongly broadens atomic transitions and their frequencies are ‘redshifted’. The second derivative method applied to the absorption spectra of the nanocell allowed the measurement of the van der Waals interaction coefficient C_3 for the ^{39}K D_1 line. It has been shown that the dipole–dipole interaction between ^{39}K atoms results in the additional ‘redshift’ at an increase of the density of atoms for the nanocell thickness $L < 100$ nm. The results obtained are important for the development of submicron devices containing free atoms.

This work was supported by the State Committee for Science, Ministry of Education and Science of the Republic of Armenia (project no. N21T-1C005).

References

[1] A. Sargsyan, G. Pichler, D. Sarkisyan, JETP Lett, **115**, 312 (2022).

Oral report

Expanded Ro–Vibrational Analysis of the Dyad Region of $^{12}\text{CD}_4$ and $^{13}\text{CD}_4$: Line Positions, Energy Levels, and Absolute Line Strengths

O. V. Gromova¹, O. N. Ulenikov¹, E. S. Bekhtereva¹, S. Bauerecker²

¹ *Research School of High-Energy Physics, National Research Tomsk Polytechnic University, Lenin av., 30, 634050, Tomsk, Russia*

² *Institut für Physikalische und Theoretische Chemie, Technische Universität Braunschweig, D-38106, Braunschweig, Germany.*

Email: gromova@list.ru

The high resolution infrared spectra of $^{12}\text{CD}_4$ and $^{13}\text{CD}_4$ were measured with a Bruker IFS125 HR Fourier transform infrared spectrometer at an optical resolution of 0.003 cm^{-1} and analyzed in the region of $800\text{--}1400\text{ cm}^{-1}$ where the ν_2/ν_4 dyads are located. The number of 5600 and 2100 transitions with $J_{\text{max}} = 31$ and $J_{\text{max}} = 26$ were assigned to the $^{12}\text{CD}_4$ and $^{13}\text{CD}_4$ isotopologues (which is more than three times higher in comparison with the number of assigned transitions known in the

literature). The subsequent weighted fit of experimentally assigned transitions was made with the Hamiltonian model which takes into account the resonance interactions between the upper (0001, F_2) and the (0100, E) vibrational states. As a result, a set of 52 fitted parameters (10 parameters of the ground vibrational state, 19 parameters of the (0001, F_2) vibrational state, 9 parameters of the (0100, E) vibrational state, and 14 resonance interaction parameters) was obtained which reproduces the positions of the initial experimental ro-vibrational transitions with the $d_{\text{rms}} = 1.8 \times 10^{-4} \text{ cm}^{-1}$ which is close to the experimental uncertainty of the recorded spectra and is about 615 times better in comparison with the reproduction of the same transition values by the use of parameters from the literature. Line strengths analysis of both isotopologues was made for the first time.

This research was supported by TPU development program Priority 2030 (project NIP/EB-010-0000-2022).

Oral report

Plasmonic Nanostructures with Laser Induced Chirality

I. A. Gladskikh, D. R. Dadadzhanov, A. Sapunova G. Alexan, R. A. Zakoldaev, T. A. Vartanyan

ITMO University, Kronverksky Pr. 49, bldg. A, St. Petersburg, 197101, Russia

Email: 138020@mail.ru

The study of complex plasmonics structures, in particular, chiral has become especially relevant in recent years. Chiral nanoparticles and their ensembles interact differently with left and right circularly polarized light. Chirality can be either a property of an individual particle or a complex of achiral particles arranged in a chiral pattern. The approaches used so far for chiral plasmonic materials fabrication were rather involved relying on the electron lithography or DNA molecules as a chiral scaffold. Here we report on a much simpler approach based on the laser-induced modification of the self-assembled achiral plasmonic nanostructures.

2D metal nanostructures with strong optical dichroism have been fabricated via a novel method based on the spectral hole burning technique. The essence of the method lies in the selective heating and reshaping of metal nanoparticles by pulsed laser irradiation with circular polarization. We have fabricated two types of samples: (i) 2D silver structures, obtained by physical vapor deposition on the dielectric substrates and (ii) 3D structures of small gold nanoparticles in porous glass. The samples were irradiated with the focused 2-nd harmonic beam of a picosecond Nd:YAG laser with circular polarization. The laser fluence varied from 8 to 50 mJ/cm².

After irradiation, both spectra of optical density and spectra of circular dichroism (CD) changed dramatically. Laser irradiation with moderate fluence leads to a decrease in optical density mainly at the irradiation wavelength. At fluences higher than 20 mJ/cm², a significant decrease in the optical density is observed at all wavelengths, which can be associated with the silver ablation from the substrate surface. The CD spectra show that transmittance was larger for probe light with circular polarization coincident with polarization of the laser irradiation. Maximum of CD spectra was close to the irradiation wavelength.

These results are in agreement with the theory of spectral hole burning. The initial state of the self-assembled films is achiral due the balance between the numbers of chiral particles of different

chirality. Irradiation with circularly polarized light leads mostly to the heating and reshaping of the particles with the particular chirality, while the particles with the opposite chirality remain unaffected. Thus, the balance is compromised and the film, as a whole, demonstrates circular dichroism. For 3D structures chirality will be induced both on the surface like in 2D structures and in the bulk. Because of that, different CD spectra were measured for different orientations of the substrate with regard to the incident probe beam direction of propagation.

The study was supported by the Russian Science Foundation grant No. 21-72-10098,
<https://rscf.ru/en/project/21-72-10098/>.

Oral report

Noise Calculation of Various Design Thermoelectric Detection Pixel for UV Single Photons Registration

A. S. Kuzanyan^{1,3}, A. A. Kuzanyan^{1,2}, V. R. Nikoghosyan¹, S. R. Harutyunyan^{1,3}

¹*Institute for Physical Research, NAS of Armenia, Ashtarak, Armenia*

²*University of California, Los Angeles, CA, USA*

³*Russian-Armenian University, Yerevan, Armenia*

Email: akuzanyan@yahoo.com

Detection pixels of single-photon thermoelectric detectors are thermal sensors that convert the heat of absorbed photons into voltage. The following noises occur in the thermal radiation sensor: Johnson, phonon, photon, load, amplifier, flickering, and contacts [1]. The last three types of noise are related to the electrical signal reading circuit and are not characteristics of the detection pixel. The thermoelectric detector does not need additional load. Therefore, load noise is eliminated. We also do not consider photon noise, since the single-photon detector must be protected from background radiation.

We present the results of calculations of Johnson and phonon noises that occur in the three-layer detection pixel of a thermoelectric single-photon detector after absorption of 3.1 – 7.1 eV (400 – 175 nm) UV photons in the detection pixel with a surface area of $2 \times 2 \mu\text{m}^2$ and various thicknesses of layers. Tungsten (W), lanthanum hexaboride (LaB_6), superconductors Nb, Pb, YBCO, and Bi-2223 were considered as absorber and heat sink materials. FeSb_2 , CeB_6 , and $(\text{La}, \text{Ce})\text{B}_6$ thermoelectrics, which have high properties at temperatures of 0.5–9 K, were considered as sensor materials, so in this temperature range the operating temperatures of the detector were chosen.

The equation for the total equivalent power of Johnson and phonon noise of the three-layer detection pixel is obtained,

$$NEP = (NEP_{jn}^2 + NEP_p^2)^{1/2} = \{[4kTA(l\rho + 2l_1\rho_1)]S^{-2}(4\sigma_s T^3 + K/l + 2K_1/l_1)^2 + [4kT^2A(4\sigma_s T^3 + K/l + 2K_1/l_1)]^{1/2}\},$$

where NEP_{jn} and NEP_p are the equivalent power of Johnson and phonon noise, k – Boltzmann constant, T – absolute temperature, A – surface area of the detection pixel, σ_s – Stefan-Boltzmann constant, l , ρ and K – thickness, electrical conductivity and thermal conductivity of the thermoelectric,

l_1 , ρ_1 and K_1 – thickness, electrical conductivity and thermal conductivity of the absorber and heat sink. Using the NEP and the thermal time constant ($\tau = C / G$, C – heat capacity, G – heat conductance) values of the detection pixel, promising designs of the detection pixel were determined.

This work was supported by the Science Committee of RA, in the frames of the research project №21T-1C088 “Sensor development of the thermoelectric single-photon detector for UV radiation taking into account thermal noise”.

References

- [1] U. Dillner, E. Kessler, H.-G. Meyer, *J. Sens. Sens. Syst.*, **2**, 85 (2013).

Oral report

Dressed States and Suppression of Dissipative Processes

G. G. Grigoryan

Institute for Physical Research, Ashtarak, 0203 Armenia

Email: gaygrig@gmail.com

It is well known that any dissipative processes lead to information loss [1]. Despite the rapid development of quantum information, the problem of suppression of dissipative processes has not been resolved to date.

If the quantum systems interact with external fields, the energy levels of these systems change and so-called dressed states are formed [2].

Dressed states are the eigenstates of the Hamiltonian, including interaction. Once these dressed states are found, the dynamics of the system are very simple. These states are very useful for qubit creation and different logic gate implementation, and have found wide application in theory [3]. However, different dissipative processes (for example, spontaneous relaxation) mix these states, leading to their destruction. Another mechanism of mixing dressed states is the nonadiabatic transition between dressed states.

In this paper, using the example of a two-level model, it is shown that by choosing the interaction parameters, it is possible to ensure that these two mechanisms compensate each other. In this way, the system becomes stable with a sufficiently long interaction time.

References

- [1] Lambropoulos, P., & Petrosyan, D. (2007). *Fundamentals of quantum optics and quantum information*. Berlin: Springer.
- [2] Тер-Микаелян М. Л. Простейшие атомные системы в резонансных лазерных полях *Успехи физических наук*. (1997). Т. 167. №. 12. с. 1249-1294.
- [3] Vitanov N. V., Rangelov A. A., Shore, B. W., & Bergmann K. (2017). Stimulated Raman adiabatic passage in physics, chemistry, and beyond. *Reviews of Modern Physics*, 89(1), 015006.

Oral report

Polaron Mechanism of Conductivity in Zinc Oxide Films

N. R. Aghamalyan¹, H. L. Ayvazyan¹, R. K. Hovsepyan¹, Y. A. Kafadaryan¹, H. G. Mnatsakanyan¹, A. R. Poghosyan¹, T. A. Vartanyan²

¹ *Institute for Physical Research, Ashtarak-2, Armenia*

² *Univ. of Information technology, Mechanics and Optics, Sankt-Petersburg, Russian Federation*

Email: apoghosyanipr@gmail.com

There is great interest in materials for one-transistor capacitive memory elements (1T1C-DRAM) based on a non-junction gate FET (GAA-JLFET) for transparent structures with high memory density. Semiconductors A^2B^6 and, in particular, ZnO are an interesting material for creating such memory cells, since the dielectric properties of ZnO films can be controlled by a donor or acceptor impurity doping. The goal of this study is the investigations of the dielectric properties and mechanisms of charge carrier transport of ZnO and ZnO:Li films in wide frequency and temperature range to demonstrate the possibility of creating a memory element that combines a capacitor and a field-effect transistor. ZnO:Li dielectric layer can be used as channel of the FET and dielectric for capacitor.

The films were obtained by the electron-beam vacuum deposition method and had a textured structure. The dielectric properties and the mechanism of charge carrier transport in ZnO films doped with an acceptor lithium impurity were studied. The dielectric properties of zinc oxide were studied in the range of 8–36°C. The frequency dependence of conductivity was studied in the range 100 Hz - 400 MHz. The frequency dependence of the capacitance was studied in the range 1 MHz - 400 MHz. Measurements of the FET parameters were carried out in the range 0 – 10 MHz. A strong dispersion of permittivity constants at low frequencies was observed, which can be attributed to interfacial relaxation. The obtained frequency dependences of the conductivity were interpreted by the various models of charge carrier transport in the framework of the theory of Mott's hopping conductivity.

The results obtained were used for creation of the single-transistor capacitive memory elements (1T1C) and field-effect transistors with floating-gate. Proposed DRAM has good potential for memory applications because it has a high reading speed; the ratio of currents in states "1" and "0" is about 10^5 , and the holding time exceeds 10 ms.

Oral report

Suppression of the Light Shift of the CPT Resonance Frequency in ^{87}Rb Atoms

M. I. Vaskovskaya, E. A. Tsygankov, D. S. Chuchelov, S. A. Zibrov, V. V. Vassiliev, V. L. Velichansky

P.N. Lebedev Physical Institute of the Russian Academy of Sciences, 119991, Moscow, Russia

Email: vaskovskayami@lebedev.ru

The light shift is one of the main factors limiting the stability of frequency standards based on the

effect of coherent population trapping (CPT). Most often, in standards of this type, a VCSEL (vertical-cavity surface-emitting laser) is used as a radiation source, and its injection current is modulated by a microwave signal. In this case, the laser radiation spectrum is polychromatic, and the light shift of the CPT resonance frequency is the sum of the shifts from each spectral component. Since the light shifts produced by different components have opposite signs the total light shift can be suppressed by the correct choice of the microwave modulation depth [1].

We studied the influence of buffer gas pressure on light-shift suppression. Buffer gas (BG) is needed to narrow CPT resonance by decreasing the coherence relaxation at the walls of a cell. The smaller is the cell the greater should be gas pressure. High BG pressure leads to the broadening of optical absorption line. We found that when BG pressure and corresponding optical linewidth exceed certain threshold values, the light shift can't be suppressed. This result is of practical importance in the production of CPT-based frequency standards with mm-scale atomic cells.

The influence of the features of the VCSEL modulation spectrum and modulation efficiency on the light-shift suppression is discussed. A method is proposed to evaluate whether a certain modulation VCSEL spectrum (even if asymmetric) provides suppression of the light shift. It is based on the calculation of the sum of light shifts from each spectral component of laser radiation.

References

- [1] M. Zhu, L.S. Cutler, 32nd Annual Precise Time and Time Interval (PTTI) Meeting, 2000.

Oral report

Magnetic Field Values Annihilating Alkali Atoms' Transitions

A. Aleksanyan^{1,2}, R. Momier^{1,2}, E. Gazazyan^{1,3}, A. Papoyan¹, C. Leroy²

¹ *Institute for Physical Research, NAS of Armenia, Ashtarak-2, 0203, Armenia*

² *Laboratoire Interdisciplinaire Carnot de Bourgogne, UMR CNRS 6303, Université de Bourgogne Franche-Comté, 21000 Dijon, France*

³ *Institute for Informatics and Automation Problems, NAS of Armenia, Yerevan, 0014, Armenia*

Email: arthuraleksan@gmail.com

Analytically, all electric dipole transitions (π , σ^+ and σ^-) between the magnetic sublevels of D_1 line of all alkali metal atoms are considered [1]. General 2×2 block Hamiltonian matrices corresponding ground and excited states are constructed. After the eigenkets and eigenvectors are calculated, we obtain "modified" transfer coefficients which depend on the nuclear spin I , the magnetic quantum number m and the magnetic field magnitude B . Transition cancellations exist only for some π transitions of each isotope where the total atomic angular momenta of ground and excited states are equal to each other ($F_g = F_e$). As a result, we obtain a unique formula that expresses the magnetic field values canceling these transitions:

$$B = -\frac{2m}{\mu_B(1+2I)} \times \frac{2\varepsilon_g\varepsilon_e}{(g_I - g_S)\varepsilon_e + \frac{3g_I - 4g_L + g_S}{3}\varepsilon_g}, \quad (1)$$

where μ_B is the Bohr magneton, m is the magnetic quantum number, I is the nuclear spin, g_I , g_S and g_L are respectively the nuclear, electronic and angular Landé factors, ε_g and ε_e are the energy

difference of the ground and excited states, and $0 \leq (-1)^{2I}m \leq I - 1/2$. These B values also correspond to the case when some of other transitions intensity reach their maximum. Furthermore, we examine the derivative of π transition “modified” transfer coefficients in order to find the magnetic field values corresponding to the maximum transition intensities.

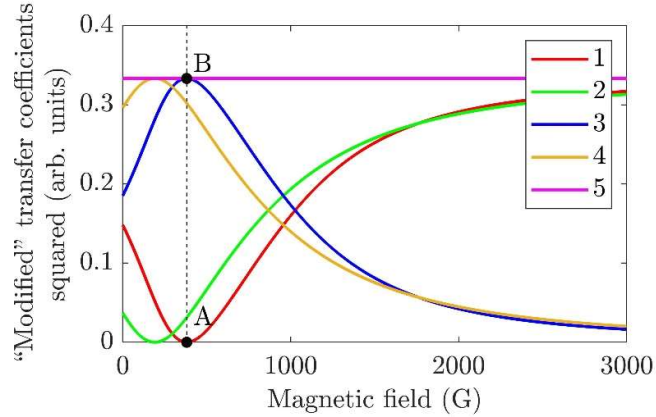


Fig. 1. ^{85}Rb D_1 line “modified” transfer coefficients squared. The vertical dashed line indicates the value $B = 380.73$ G that corresponds to the cancellation of the transitions (point A) and coincides with the maximum of transitions (point B). Lines 1 and 2 correspond to the transfer coefficients for $m = -2$ and $m = -1$ values respectively, where $F_g = F_e$. Lines 3 and 4 correspond to the transfer coefficients for $m = -2$ and $m = -1$ values respectively, where $F_g \neq F_e$. “Guiding” transition coefficient squared (line 5) corresponds to $m = -3$.

For matrices of dimension higher than 2×2 , formulas exist but are heavy, thus we have performed numerical calculations. We have analyzed $5^2S_{1/2} \rightarrow 5^2P_{3/2}$ and $5^2S_{1/2} \rightarrow 6^2P_{3/2}$ transition cancellations of the ^{85}Rb and ^{87}Rb alkali metal [2,3]. The accuracy of the magnetic field B values is limited solely by the uncertainty of the physical quantities involved in our calculations.

References

- [1] P. Tremblay, A. Michaud, M. Levesque, S. Thériault, M. Breton, J. Beaubien, and N. Cyr, Phys. Rev. A, **42**, pp. 2766–2773, (1990).
- [2] A. Aleksanyan, R. Momier, E. Gazazyan, A. Papoyan and C. Leroy, J. Opt. Soc. Am. B, **37**, 11, pp. 3504-3514 (2020).
- [3] R. Momier, A. Aleksanyan, E. Gazazyan, A. Papoyan and C. Leroy, J. Quant. Spectrosc. Radiat. Transf., **257**, p. 107371 (2020).

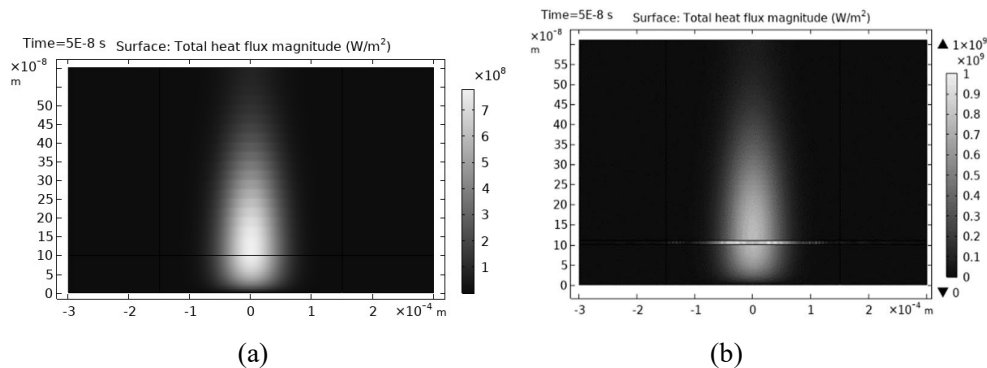
Temperature Dynamics of Laser Heating of Composites "Substrate/Amorphous Silicon Film" and "Substrate/Gold Nanoparticles/Amorphous Silicon Film"

A. Fedotov, Y. Tsitavets, I. Dadenkov

Belarusian State University, Nezalezhnasci Ave. 2, Minsk 220030, Belarus

Email: fedotov.alejandro@gmail.com

Ultrashort pulse lasers have proven to be effective in material processing, offering many advantages over long pulses: precise micromachining with a minimum heat affected zone that can be achieved due to small thermal diffusion lengths associated with ultrashort pulses. Laser ablation and metal melting are used to manufacture microelectronics, and numerical simulations provide a better understanding of these processes. The use of short and ultra-short pulses in material processing requires a deviation from traditional heat transfer models. In this work we consider a finite element model of laser heating of nanocomposites in two configurations: "substrate / amorphous silicon film" and "substrate / gold nanoparticles / amorphous silicon film". The proposed nanocomposites are supposed to be promising materials for selective laser crystallization of amorphous silicon. The thickness of amorphous silicon was supposed to be of 100 nm, the thickness of the gold layer was 10 nm, laser pulse duration was 10 ns with a fluence of 10^{-2} J/cm². The temporal and spatial distributions of temperature and heat flux during laser heating of above-mentioned composites by nanosecond laser pulses are studied based on the developed one- and two-temperature models [1]. It is established that the influence of the gold layer in composites causes a more uniform redistribution of heat in the amorphous silicon layer, which makes it possible to expect an increase in the quality of crystallized silicon. Two-temperature models for heating the gold layer and silicon, are supplemented by the equation for the dynamics of charge carriers. The spatial distribution of heat flux is shown in the figure for the composites: (a) «substrate/amorphous silicon film» and (b) «substrate/gold nanoparticles/ amorphous silicon film» after 50 ns from the beginning of irradiation.



Reference

[1] P. Bresson et al. Phys. Rev. B. **102**, P. 155127 (2020)

Atomic Cells Production by Laser Technology

D. S. Chuchelov¹, A. B. Egorov², E. A. Tsygankov¹, V. V. Vassiliev¹, M. I. Vaskovskaya¹, V. L. Velichansky^{1,3}, S. A. Zibrov¹

¹*P. N. Lebedev Physical Institute, Russian Academy of Sciences, 119991 Moscow, Russia*

²*Prokhorov General Physics Institute of the Russian Academy of Sciences, 119991 Moscow, Russia*

³*National Research Nuclear University MEPhI (Moscow Engineering Physics Institute), 115409 Moscow, Russia.*

Email: factorialzero@gmail.com

Many types of quantum sensors are based on spectral and metrological properties of alkali atoms. Of late, particular interest is in the development of compact atomic clocks, magnetometers, gyros which use miniature cells. The cells localize an ensemble of atoms, protect it from external perturbations, and pass pump and probe laser light. We present an original technique of a cell-body production by laser welding, filling of a cell with alkali metal and buffer gases, and laser sealing. We describe pros and cons of the developed technology and compare it with other cell fabrication methods. We produce cylindrical and cubic-shaped cells with characteristic dimensions of a few millimeters. Both walls and windows of cells are made of glass. One of the problems related to the CO₂ laser sealing is the high temperature of melted glass, which leads to the release of gases dissolved in the glass. Part of this gas is encapsulated which might change metrological characteristics of a cell. To control the residual pressure whose minimizing is important for compact optical atomic clocks we take Doppler-free spectra of D₁ line alkali atoms [1,2]. We found that the ratio the saturation resonance area to its peak depends on buffer gas pressure linearly up to 100 mTorr. We explain the shape of the observed resonances and explain the elastic collisions broadening of the resonance. Another problem of laser sealing refers to cells filled with buffer gases needed in chip scale atomic clock. An increase of the mean cell temperature during the sealing causes some of the buffer gas to escape. We check the resulting pressure of buffer gases by measuring the frequency of the resonance of coherent population trapping [3]. Thus, to a large extent we solved the problems of heating that accompanies laser sealing. The cells produced by the developed technology are successfully used in many applications.

References

- [1] Thornton D. E., Phillips G. T., Perram G. P. Optics Communications. – 2011. – T. 284. – №. 12. – C. 2890-2894.
- [2] Smith P. W., Hänsch R. Physical Review Letters. – 1971. – T. 26. – №. 13. – C. 740.
- [3] Vaskovskaya M. I. et al. Optics express. – 2019. – T. 27. – №. 24. – C. 35856-35864.

Nanometric-Thin K Vapor Cell Used as a Large-Range Magnetometer

R. Momier^{1,2}, A. Sargsyan², A. Tonoyan², M. Auzinsh³, D. Sarkisyan², A. Papoyan² and C. Leroy¹

¹ *Laboratoire Interdisciplinaire Carnot de Bourgogne, UMR CNRS 6303, Université Bourgogne Franche-Comté, 21000 Dijon, France*

² *Institute for Physical Research, NAS of Armenia, Ashtarak-2, 0203 Armenia*

³ *Department of Physics, University of Latvia, Rainis boulevard 19, LV-1586 Riga, Latvia*

Email: rodolphe.momier@u-bourgogne.fr

Alkali atoms are commonly used in atomic physics for a number of reasons, the main one being the simplicity of their electronic structure. Relatively cheap lasers are available for the main optical transitions (D lines) of most alkali atoms making them convenient to study experimentally, mainly in the domain of magnetometry [1, 2]. Potassium 39 (^{39}K) is an interesting candidate for such experiments, since it has the smallest characteristic value $B_0 = A_{hfs}/\mu_B \simeq 170^{++}$ G (where A_{hfs} is the ground state's magnetic dipole interaction constant) characterizing the decoupling of J and I and therefore the establishment of hyperfine Paschen-Back (HPB) regime [3, 4]. Probing a ^{39}K vapor with a circularly polarized laser while applying a strong enough (> 200 G) magnetic field oriented along the propagation direction of laser allows to record an absorption spectrum in which only 8 spectrally resolved Zeeman transitions (4 for each circular polarization σ^\pm) are visible, while the probabilities of the 16 remaining transitions tend to zero. Complete spectral resolution is obtained thanks to the thickness of the vapor cell, allowing almost complete cancellation of the Doppler broadening [5]. We present a method that allows to measure the magnetic field with micrometer spatial resolution based on the recorded spectra in the range 0.1 – 10 kG with a cell of thickness $L = 120 \pm 5 - 390 \pm 5$ nm, which is relevant in particular for the determination of magnetic fields with a large gradient (up to 3 G/ μm). The experimental results are verified by theoretical calculations.

References

- [1] D. Budker *et al*, *Rev. Mod. Phys.* **74**, p. 1153 (2002).
- [2] E. Klinger *et al*, *Appl. Opt.* **59**, p. 2231 (2020).
- [3] B. A. Olsen *et al*, *Phys. Rev. A* **84**, 063410 (2011).
- [4] A. Sargsyan *et al*, *Opt. Lett.* **37**, p. 1379 (2012).
- [5] D. Sarkisyan *et al*, *Opt. Comm.* **200**, p. 201 (2001).

Terahertz Generation Using a Nitrogen-Doped Diamond Photoconductive Antenna

V. V. Bulgakova¹, P. A. Chizhov¹, M. S. Komlenok¹, V. V. Kononenko¹, V. V. Bukin¹, A. A. Ushakov¹, A. A. Khomich², A. P. Bolshakov¹, V. I. Konov¹, S. V. Garnov¹

¹ *Prokhorov General Physics Institute of the Russian Academy of Sciences, Vavilov Street 38,
Moscow, Russia*

² *Kotelnikov Institute of Radio Engineering and Electronics RAS, Fryazino, Russia*

Email: vbulgakova573@gmail.com

The most common and promising source of terahertz (THz) radiation is a photoconductive antenna (PCA). These sources are relatively powerful broadband pulsed emitters with high ponderomotive potentials [1], which can be used to solve a number of physical problems, such as the Rydberg atom ionization [2]. In this work, the diamond was chosen as the substrate of the PCA. This material has great prospects in this area, since it has a high breakdown field (10 MV/cm [3]), which makes it possible to boost the amplitude of a THz field via to increase the bias voltage applied; as well diamond is transparent in the THz region [4]. Despite the advantages, diamond was not used as a substrate for a PCA, since its band gap is 5.46 eV, which requires deep ultraviolet radiation for efficient single-photon excitation of the electronic subsystem. It was proposed to introduce nitrogen to create optical defects into the diamond lattice to form relatively low-energy transitions from defect levels to the conduction band for the implementation of photoconductive diamond-based antennas.

In this work, generation of terahertz radiation was obtained for the first time using photoconductive antennas based on nitrogen-doped HPHT and CVD diamond. Different concentrations of nitrogen in diamonds made it possible to obtain a saturation fluence from the very high (approximately 12000 $\mu\text{J}/\text{cm}^2$) to the quite low (approximately 40 $\mu\text{J}/\text{cm}^2$) for dielectric materials using a pump by the second harmonic of a Ti:sapphire laser. Using time-domain spectroscopy technique the temporal dependency of THz electric field was measured. The emitted THz pulses had a typical large aperture PCA asymmetrical form with a low-frequency part. It was found that the duration of the THz pulse depends on the nitrogen concentration in diamond. The PCA based on nitrogen-doped HPHT and CVD diamond and CVD-ZnSe are compared.

References

- [1] X. Ropagnol, M. Khorasaninejad, M. Raesizadeh, et al., *Optics Express* **24**, 11299-11311, (2016).
- [2] R. R. Jones, D. You, and P. H. Bucksbaum, *Phys. Rev. Lett.* **70**, 1236, (1993).
- [3] H. Yoneda, K.-I. Ueda, Y. Aikawa, et al., *Appl. Phys. Lett.* **66**, 460, (1995).
- [4] V. Kubarev, *Nucl. Instrum. Methods Phys. Res. Sect. A* **603**, 22-24, (2009).

Oral report

An Asymmetric Version of the Second Demkov-Kunike Level-Crossing Model

T. A. Shahverdyan^{1,2}, A. M. Ghazaryan^{1,2}, and A. M. Ishkhanyan^{1,2}

¹*Russian-Armenian University, Yerevan, 0051 Armenia*

²*Institute for Physical Research, Ashtarak, 0204 Armenia*

Email: ghazaryanastghik2.7@gmail.com

We present a new time-dependent two-state model that can be viewed as an asymmetric version of the second Demkov-Kunike model. The model describes a constant-amplitude level-crossing field configuration, for which the frequency detuning changes within a finite interval. A peculiarity of the configuration is that the level crossing occurs asymmetrically in time. The general solution of the problem is given by two independent irreducible linear combinations of the Gauss hypergeometric functions. We rewrite the solution in terms of the associated quasi-energies and discuss the transition probability for the case when the system starts from the first quasi-energy state.

Oral report

Combined Method of Laser and Chemical Treatment of Painted Gypsum Base-Relief

A. V. Vasileva¹, A. K. Kareva², V. A. Parfenov¹

¹*St. Petersburg State Electrotechnical University "LETI" named after V.I. Ulyanova, 5 Prof. Popova street, 197022, St. Petersburg, Russian Federation*

²*St. Petersburg State Academy of Art and Industry named after A.L. Stieglitz, 13 Solyanoy pereulok, 191028, St. Petersburg, Russian Federation*

Email: anastasiastru@mail.ru

The work examined a fragment of the 18th-century bas-relief from the courtyard facade of the St. Petersburg Academy of Arts building. UV shooting and energy-dispersive X-ray spectroscopy showed that there were several paint layers on the surface of the bas-relief, however, only the inner layers of terracotta-colored paint were of historical value. The historical layers were covered with several layers of white paint and gypsum, as the result of repeated renovations of the bas-relief in different historical periods. The traditional cleaning method using chemical solvents did not demonstrate the desired result, since the surface layer of white paint was highly resistant to chemical solvents. Therefore, it was decided to carry out trial clearings using laser cleaning technology.

Laser cleaning is actively used today in the restoration of Cultural Heritage and shows effective results in cleaning of stone monuments and metal objects [1]. The pulsed solid-state Nd:YAG laser with a wavelength of 1064 nm is most widely used [1, 2]. In addition to cleaning metal and stone objects, there are known examples of use Nd:YAG lasers in the restoration of wall paintings and stone surfaces with decorative paint layers [3], as well as gypsum objects covered with black gypsum crusts

[4, 5], which made it possible to talk about the potential use of this type of laser to solve the problems of this study.

As a result of the research, a combined method was developed for cleaning a gypsum bas-relief from surface paint layers using a chemical solvent of dimethyl sulfoxide in combination with laser cleaning technology. The laser action mode for the white paint was chosen, in which the paint surface was destructurized, and then the solvent penetrated deep and reacted with needless surface layers. Comparative analysis with the area cleaned by the traditional method showed that the area cleaned by the combined cleaning method had a more uniform color without visible surface damage.

References

- [1] M. Cooper, “Laser Cleaning in Conservation”, Butterworth-Heinemann, UK, 1998.
- [2] S. Siano, J. Agresti, I. Cacciari, et. al., Applied Physics A **106**, 419 (2012).
- [3] “Science and Art: The Painted Surface. 1st edition”, Ed: A. Sgamellotti, B. G. Brunetti, C. Miliani, The Royal Society of Chemistry, UK, 2014.
- [4] S. Siano, M. Giamello, L. Bartoli, et. al., Laser Physics **18 (1)**, 1 (2008).
- [5] G. Grammatikakis, K. D. Demadis, K. Melessanaki, et. al., Studies in Conservation **60 (1)**, S3–S11 (2015).

Oral report

Surface Enhanced Raman Scattering by Dye Molecule on Silver Substrates

M. Goncalves¹, A. Melikyan², H. Minassian³, P. Petrosyan⁴

¹ *Ulm University, Ulm, Germany,*

² *Institute of Applied problems of Physics, NAS of Armenia,*

³ *Yerevan Physics Institute*

⁴ *Yerevan State University*

Email: petrosyanpetros00@gmail.com

We consider theoretically the surface enhanced Raman scattering (SERS) from R6G molecule placed in the gap of Ag dimer. The Ag nanoparticles (NP) are modeled as nanospheroids and nanorods with different aspect ratios (AR) of 1.5 – 14. The dye molecule is modeled as a small solid sphere with the polarizability coinciding with that measured for R6G molecule. The calculations of the SERS enhancement factor (EF) were performed by finite element method (FEM) exploiting COMSOL Multiphysics software. It is shown that the EF is not sensitive with respect to the Ag particle volume and is mostly determined by the AR. The largest value of EF – 5×10^{13} at $\lambda=540$ nm was obtained when the surface plasmon (SP) wavelength of coupled NPs approaches the dye molecule absorption resonance (Resonance SERS) for AR of 3.0 for all considered volumes of dimers. The SERS was also studied for single Ag NP and the value of 1.5×10^{11} was obtained for EF, clearly demonstrating the important role of hot-spot effect. Another important outcome of our study is revealing the quadrupole

SP resonance in dimer at shorter wavelengths. This effect along with dipole SP resonance allows extension of wavelength range with high values of EF.

Oral report

Narrow-Band and Bright Fluorescence of Silver Nanoclusters in a Plasmonic Cavity

A.S. Gritchenko¹, A.S. Kalmykov¹, B.A. Kulnitskiy^{2,3}, Y.G. Vainer¹, Shao-Peng Wang⁴, B. Kang⁴, P.N. Melentiev¹ and V.I. Balykin¹

¹*Institute of Spectroscopy RAS, Moscow, Troitsk, Russia.*

²*Technological Institute for Superhard and Novel Carbon Materials, Moscow, Troitsk, Russia*

³*Moscow Institute of Physics and Technology, Moscow reg., Dolgoprudny, Russia*

⁴*State Key Laboratory of Analytical Chemistry for Life Science and Collaborative Innovation Center of Chemistry for Life Sciences, School of Chemistry and Chemical Engineering, Nanjing University, Nanjing, P. R. China*

Email: gritchenkoant@gmail.com

Ultra-bright and narrow-band nano-localized light sources are now of great demand in a variety of research areas, from quantum optics and communications to biosciences. However, nano light sources, usually show low emission cross-sections and wide fluorescence spectrum, which is the limiting factor for their use in many applications. Thus, the creation of nano-localized radiation sources is one of the required tasks of modern photonics.

In the present work, we have created and investigated a novel, ultra-bright and narrow-band nano-localized light source based on a silver nanocluster in a plasmonic cavity. The fluorescence cross-section of created light source is on the order of $\sigma \sim 10^{-14} \text{ cm}^2$, which is comparable to the largest fluorescence cross-sections of dye molecules and quantum dots, and enables a light source with a record high intensity known only for plasmon nanolasers. Optical properties of the silver nanocluster in gap plasmon cavity, measured in this work, reveals cavity-induced mechanism of line narrowing and fluorescence lifetime shortening [1].

A major advantage of the created nano-localized radiation source is its relatively simple fabrication by self-assembly at the atomic level. These nano-localized light sources can find application in the area of nanophotonics, including the fabrication of optical devices on a chip. In addition, such nanoprobe are in high demand in medical and bioscience applications.

References

- [1] A. S. Gritchenko, A. S. Kalmykov, P.N. Melentiev, *et al.* (2022). *Nanoscale*, 14(27), 9910, (2022).

Synthesis, Structure, Magnetic and Magnetic Heating Properties of Carbon Coated Fe-Fe₃C Nanoparticles

H. Gyulasaryan¹, E. Myrovali², G. Chilingaryan¹, E. Papadopoulou³, N. Tetos³, A. Ginoyan¹, A. Makridis², N. Sisakyan¹, M. Spasova³, M. Farle³, M. Angelakeris², A. Manukyan¹

¹ *Institute for Physical Research of National Academy of Sciences, Armenia*

² *Physics Department, Aristotle University of Thessaloniki, Greece*

³ *Faculty of Physics and Center of Nanointegration (CENIDE), University of Duisburg-Essen, Germany*

Email: gharut1989@gmail.com

Magnetic nanomaterials are widely used in biomedicine due to their unique magnetic properties, making them a suitable candidate for diagnostic and therapeutic applications, in particular in magnetic hyperthermia. Magnetic hyperthermia is generally understood as a local (cellular) temperature increase up to 45 °C in malignant cells based on the heating effect of localized magnetic nanoparticles (MNPs) in cancerous tissue under alternating magnetic fields (AMF) to achieve selective damage of tumor tissue. Iron based magnetic nanoparticles with a core-shell architecture offers controllable and tunable magnetic properties and due to their low toxicity are efficient candidates in magnetic fluid hyperthermia of cancer cells.

Carbon-coated iron-cementite (Fe-Fe₃C) magnetic nanoparticles in a carbon matrix were synthesized by a solid-phase pyrolysis of ferrocene (FeC₁₀H₁₀). For better understanding the output materials magnetic heating properties dependencies on the parameters of pyrolysis, the set of samples were prepared at various temperatures (700°C, 750°C, 800°C, 850°C, 900°C, 1000°C) with different pyrolysis time for each sample (5, 15, 45 and 120 minutes). By varying the pyrolysis time and temperature, one can change the concentration of Fe and Fe₃C in metal nanoparticles, which leads to a change in the magnetic characteristics and magnetic heating properties of the nanoparticles.

The heating efficiency of synthesized samples was evaluated by preparing aqueous solutions of 6.5 mg/ml concentration and exposing them in AC magnetic field with parameters 375 kHz/60 mT. The SLP (Specific Loss Power) values of the samples prepared by the pyrolysis with various duration and temperature are given on the table.

Temperature, °C	SLP, W /g			
	5 min	15 min	45 min	120 min
700	88	83	128	263
750	163	291	350	314
800	260	222	260	179
850	234	211	200	153
900	167	209	124	126
1000	148	127	120	102

This work was supported by European Union's Horizon 2020 research and innovation programme under grant agreement No 857502 (MaNaCa).

Oral report

Influence of Buffer Gases on the Quality Factor of CPT-Resonance in ^{87}Rb : Ar and Ne vs N_2

K. M. Sabakar^{1,2}, M. I. Vaskovskaya¹, D. S. Chuchelov¹, E. A. Tsygankov¹, S. A. Zibrov¹,
V. L. Velichanskiy^{1,2}

¹ *The P.N. Lebedev Physical Institute of the Russian Academy of Sciences, Moscow, Russia*

² *National Research Nuclear University MEPhI (Moscow Engineering Physics Institute), Moscow, Russia*

Email: kirill_sabakar98@mail.ru

Miniature frequency standards are widely used nowadays for satellite geopositioning systems, Earth surface mapping, synchronization in high-speed data transmission centers, etc. Atomic clocks based on coherent population trapping (CPT) resonance are prospective due to simultaneous miniaturization and enhancement of frequency stability [1]. The essential unit of such clocks is an atomic cell with alkali metal vapor. Atomic clocks short-term frequency stability depends on contrast and width of CPT signal.

CPT linewidth is determined by coherent superposition lifetime. Buffer gas added to cell decreases relaxation on the walls, therefore the CPT-resonance narrows. Filling with only one kind of buffer gas causes strong temperature dependence of CPT frequency [2], thus binary buffer gas mixtures with opposite temperature coefficient signs are used. The most commonly used mixture is Ar+N₂. A distinctive feature of nitrogen is the fluorescence quenching [3] that is considered to be useful for enhancing coherence lifetime.

The result of present work is that fluorescence quenching decreases CPT contrast and frequency stability. In noble gases (Ar, Ne) effect of mixing in excited state increases contrast. Experimental comparison of CPT contrast and quality parameter (contrast to width ratio) in cw-mode has been carried out for cells filled with N₂, Ar, Ne and Ar+N₂, Ar+Ne mixtures at pressures of 30, 60 and 90 Torr. We've found that contrast of resonance in N₂ is lower than in Ne and Ar, and the higher buffer gas pressure is, the higher difference in contrast between Ne/Ar and N₂ is. The quality parameter in Ne and Ar is also superior to that in N₂ at pressure above 30 Torr. Comparing Ar+N₂ and Ar+Ne mixtures revealed that maximum contrast in noble gases mixture is 2 times higher than in Ar+N₂, quality parameter is 1.5 times higher. The experiment demonstrates negative influence of fluorescence quenching and positive influence of mixing in excited state on CPT resonance contrast and quality parameter. Right choice of buffer gas mixture and partial pressures that takes into account our experimental results may improve frequency stability of atomic clocks.

References

- [1] J. Kitching, *Applied Physics Reviews* **5**, 031302 (2018).
- [2] J. Vanier et al., *Journal of Applied Physics* **53**, 5387 (1982).

[3] A. Sieradzan, F.A. Franz, *Physical Review A* **25**, 2985 (1982).

Oral report

LiNbO₃:Tm³⁺ Crystal: Material for Radiation Balanced Laser

N. Mkhitarian^{1,2}, G. Demirkhanyan^{1,2}, N. Kokanyan^{3,4}, M. Aillerie³, E. Kokanyan^{1,2}

¹*Institute for Physical Research, National Academy of Sciences of Armenia, Ashtarak-2, 0203, Armenia*

²*Armenian State Pedagogical University after Kh. Abovyan, 17, Tigran Mets Ave., Yerevan, 0010, Armenia*

³*Université de Lorraine, Laboratoire Matériaux Optiques, Photonique et Systèmes, Metz, France*
⁴*Laboratoire Matériaux Optiques* ⁴*Department of photonics, LMOPS, CentraleSupélec, 57220, Metz, France*

Email: nune.mkhitarian@gmail.com

The spectra of the absorption and emission cross sections of the LiNbO₃:Tm³⁺ crystal in the wavelength range 1650–2000 nm at room temperature were obtained. The possibilities of obtaining radiation-balanced (RB) generation on the crystal under study are estimated. The parameters characterizing the optimal RB generation of the LN:Tm³⁺ crystal at a wavelength of 1852 nm with pumping at 1837 nm are determined from the absorption and emission spectra. With the specified parameters, the optimal values of the gain and efficiency of RB generation are found, respectively, $F_{\text{gain}} \cong 0.8 \times 10^{-22} \text{ cm}^2$ and $F_{\text{eff}} \cong 0.4 \times 10^{-22} \text{ cm}^2$.

The results obtained indicate that the LN:Tm³⁺ crystal, having a sufficiently high cooling efficiency coefficient, is quite competitive in this parameter with LN:Er, ZBLANP:Yb, and Rb₂NaYF₆:Yb [1-3] for use in optical cooling systems, as well as with the Rb₂NaYF₆:Yb [3] crystal for RB generation.

References

- [1] G.Demirkhanyan, E.Kokanyan et al. to be published
- [2] C. W. Hoyt, M. Sheik-Bahae, R. I. Epstein, B. C. Edwards, J. E. Anderson, *Phys. Rev. Lett.* **85**, 3600-3603 (2000).
- [3] G. Nemova, R. Kashyap. *Rep. Prog. Phys.*, **73**, 086501-21 (2010).

*Abstracts of
Poster Reports*

Optical Techniques for the Study of DNA–porphyrin Interactions

L. Aloyan, Y. Dalyan

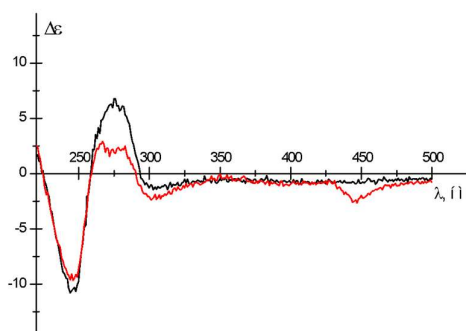
Molecular Physics Department, Yerevan State University

Email: aloyan@ysu.am

Complexation between a ligand molecule and a nucleic acid leads to optical changes in absorption and circular dichroism spectra, that can be used to monitor the binding process. As these host-drug interactions frequently involve a reversible mechanism, a determination of the equilibrium binding constant can provide insight into the nature and strength of the underlying intermolecular events. Analysis of the induced spectral effects can also reveal considerable detail about the host-drug stoichiometry, binding site size, and the thermodynamics of complex formation.

In this work, we study water-soluble cationic 4-N meso-tetra-butyl-pyridyl porphyrin and its Zn-containing analog. The porphyrins absorption Soret band (near 430 nm) was used to monitor interactions of investigated these porphyrins with duplex DNA. The addition of DNA in a solution containing a constant concentration of porphyrins results in a hypochromic effect and bathochromic (red) shift of this absorbance band for all complexes. The isosbestic point is present only at definite relative concentrations of added DNA for complexes with metal-free porphyrins. It has been suggested that more than one binding mode, in this case, is carried out. Whereas absorption spectra of complexes DNA with Zn-containing porphyrins characterized by clearly observed isosbestic point corresponded to one binding mechanism. It is significant that all results received from absorption spectroscopy are shown the best correlation with circular dichroism data. Binding parameters (K_b , n) were calculated from titration data according to the McGhee and von Hippel model.

The method of circular dichroism is based on the fact that optically active substances absorb left and right circularly polarized light differently. The high sensitivity of CD spectra to changes in molecules makes this method practically indispensable for studying the conformational transformations of molecules during the formation of complexes with ligands. The porphyrins studied in this work, as



symmetrical planar molecules, do not have natural optical activity and have zero dichroism in the entire range of electronic transitions. However, upon binding to DNA, or as a result of self-organization, porphyrins acquire asymmetry and become optically active, which can lead to the appearance of new bands in the CD spectra in their absorption region. It is known that DNA complexes with porphyrins are characterized by two CD bands (see Fig.). In presented figure CD spectra obtained in 0.1 BPSE buffer for DNA (UV region) and TBuP4/DNA complex (visible region). Band 220-

310 nm - coincides with the band of natural DNA CD, and the 400–470 nm band in the visible region is the porphyrin-induced CD band, coincides with the Soret absorption region, where DNA is transparent. Numerous studies show that analysis of the sign of the induced CD spectrum allows one to draw a conclusion about the type of porphyrin binding to DNA.

In summary, a comparison of the result obtained by CD and absorption spectrophotometry reveal that: the cationic meso-tetra-(4-N-butylpyridil) porphyrin (TBuPyP4) bind with duplex DNA by an

external and internal (intercalation) modes while their Zn-containing metallocomplexes bind only by external binding mode.

Poster report

Effect of γ -Irradiation on the Semitransparent Gray Color Obsidian in the 5 to 500 kGy Range

N. R. Aghamalyan, I. A. Gambaryan, E. A. Kafadaryan, M. N. Nersisyan,
H. T. Gyulasaryan, G. N. Chilingaryan

Institute for Physical Research, NAS of Armenia, Ashtarak, Armenia

Email: natagham@gmail.com

Obsidian, being a natural aluminosilicate glass of volcanic origin, consists of $M_2O-Al_2O_3-SiO_2$ ($M = Na, K$ and Ca) and contains various elements present in major (> 1 wt%), minor (0.1–1.0 wt%) and trace (< 0.1 wt%) amounts included in the silicate network during the glass formation. Obsidian can also contain a significant amount of water both in the form of OH groups and in the form of molecular water, which strongly influence its physical and chemical properties, as well as crystalline inclusions (the so-called microlites, up to 1–5 wt%) in glass matrix. The color of the glass depends upon the presence of various metals together with the circumstances of its formation, but obsidian is typically black or grey and is sometimes banded. Semitransparent gray color obsidian samples (bulk and powder) were irradiated at room temperature by Co^{60} radiation source with the γ -photon average energy of 1.25 MeV and with different doses from 5 to ~ 500 kGy. It is known that γ -irradiation influences on the optical properties of glass materials depending on the composition as well as due to the presence of defects in the glass matrix. Analysis of obsidian samples were carried out by the absorption and reflection spectroscopy in the UV, visible and IR ranges, as well as EPR measurements for characterization of semitransparent gray color obsidian.

Poster report

Formation of Ce^{3+} Luminescence Bands in YAG:Ce Crystals

T. I. Butaeva, K. L. Hovhannesian, A. V. Eganyan, A. G. Petrosyan

Institute for Physical Research, Armenian National Academy of Sciences, Ashtarak-2, 0203 Armenia

Email: tbutaeva@gmail.com

Spectral and structural features that affect the formation of Ce^{3+} luminescence bands in YAG:Ce garnet scintillation crystals are considered. The energy levels of the $^2F_{5/2}$ and $^2F_{7/2}$ multiplets of the 4f shell of Ce^{3+} ions occupying dodecahedral and octahedral sites of the host lattice have been determined. Participation of Ce^{3+} ions in regular and octahedral sites (Ce^{3+}_{Al}) [1, 2] in the structure of luminescence bands is shown and the multicenter structure of interconfigurational $4f \leftrightarrow 5d$ transitions

of Ce^{3+} ions is determined. Both the activator concentration and the sample volume change the shape and the emission maximum of YAG:Ce crystals. The multicenter structure of the absorption and luminescence bands of Ce^{3+} ions leads to a significant scatter of experimental data in determining the position of absorption and luminescence bands. The relative intensity of different centers of Ce^{3+} ions will determine the maximal position of the absorption and luminescence bands, while the width of these bands will be determined by the quantity of centers. The listed parameters, in turn, depend on the concentration of the activator, but may also be affected by the crystal growth method.

This work was supported by the State Committee of Science of the Ministry of Education and Science of the Republic of Armenia (project 21AG-1C030).

References

- [1] V.Babin, V.V.Laguta, A.Makhov, *et al. Nuclear Science, IEEE*, **55**, 3, 1156 (2008).
[2] T. Butaeva, I. Ghambaryan, M. Mkrtychyan., *Optics and Spectroscopy, ISSN 0030-400X*, **118**, 2, 247 (2015).

Poster report

Depth Spectroscopic Analysis of the YAG - Yb^{3+} Ceramics

G. Demirkhanyan,^{1,5} B. Patrizi,^{2*} R. Kostanyan,^{1,6} J. Li,⁴ A. Pirri,³ Y. Feng⁴, T. Xie,⁴
Zh. Yang,⁴ M. Vannini,² M. Becucci,⁶ D. Zargaryan,¹ G. Toci²

¹ Institute for Physical Research (IPR) of Armenian National Academy of Sciences;

² Istituto Nazionale di Ottica, INO, Consiglio Nazionale delle Ricerche, CNR, Italy;

³ Istituto di Fisica Applicata "Carrara", IFAC, CNR, Italy;

⁴ Shanghai Institute of Ceramics, Chinese Academy of Sciences, China;

⁵ Armenian State Pedagogical University (ASPU), Armenia;

⁶ Università di Firenze, Italy;

⁷ National Academy of Sciences of Armenia, Armenia;

Email: gdemirkhanyan@gmail.com

This paper presents the results of a detailed spectroscopic analysis of the low-temperature absorption and emission spectra of 10 at.% Yb:YAG ceramics. Based on the analysis of the temperature dependences of individual spectral lines (from 10 K to 300 K), as well as a joint analysis of the Raman spectra and temperature-resolved absorption and emission spectra, the wavelengths of zero-phonon lines and their phonon satellites are determined. As a result, a two-center model of an impurity ion is proposed, namely it is assumed that most of the ytterbium ions replace yttrium ions in dodecahedral sites (c-site), and a small part replaces aluminum ions in octahedral sites (a - site), i.e. $\{Y_{3-x}Yb_x\}[Al_{2-y}Yb_y]Al_3O_{12}$ at $x + y = 0.3$. Estimates made on the basis of Strocka's empirical formula [1], taking into account the value of the lattice parameter of the test sample is equal to 12.0006\AA [2], as well as the error of the Strocka's formula, 0.005\AA , showed that $0.2974 \leq x \leq 0.3$ and therefore, $y \leq 0.0026$.

The energies of the Stark levels of Yb^{3+} ions were determined both in the c- and a-positions. The wave functions of Stark states are constructed in JLSM representation (J, L and S are total, angular and spin

moments, MJ is projection of J). A standard Judd-Ofelt analysis is carried out and the intensity parameters are determined, and the main spectroscopic characteristics are calculated.

Acknowledgments

This work was supported by the joint program between the Ministry of Education, Science, Culture and Sports of the RA and the National Research Council of Italy (Project “Investigation of the spectroscopic and kinetic properties of mixed composition transparent ceramics doped with rare earth ions for laser applications, grant 19IT-005).

References

- [1] W. Strocka, B., Holst, P. Tolksdorf, *Philips J. Res.*, vol. 33, pp. 186–202 (1978).
[2] G. Toci, A. Pirri, B. Patrizi, et al. *Ceram. Int.*, vol.46, N11, pp. 17252–17260 (2020)

Poster report

Investigation of YAG:Pr,Ca Scintillator Crystals Annealed in Air

M. V. Derdzyan¹, K. L. Hovhannesian¹, S. N. C. Santos², G. R. Asatryan³, C. Dujardin²,
A. G. Petrosyan¹

¹*Institute for Physical Research, National Academy of Sciences of RA, 0204 Ashtarak-2, Armenia*

²*CNRS, Institut Lumière Matière, Université de Lyon, Université Claude Bernard Lyon 1, F-69622
Villeurbanne, France*

³*Ioffe Institute, St. Petersburg, 194021, Russia*

Email: mderdzyan@gmail.com

Heat treatment in various media is widely applied to garnet scintillators to modify the valence state of activators or to control the defect structure, for better performance [1].

In this work YAG:Pr,Ca scintillator crystals grown by Bridgman were further submitted to air-annealing. The process leads to appearance of a strong absorption in the 300-600 nm range with a noticeable band at ~380 nm attributed in Ref. [1] to Pr⁴⁺. A slight reduction in intensities of f-f lines of Pr³⁺ in the infrared (³H₄ → ¹G₄ transition) indicates a low efficiency of Pr³⁺ to Pr⁴⁺ conversion. No related to Pr⁴⁺ spectra could be found using the EPR method at 9.35 GHz frequency in magnetic fields up to 13 KG at 4.2 K. The radioluminescence spectra of YAG:Pr,Ca show emission of the 5d-4f transitions of Pr³⁺ at 325 nm and a shoulder around ~380 nm [1,2], along with the 4f-4f transitions at 488 nm (³P₀ → ³H₄), 505 nm (³P₂ → ³H₅), and 538 nm (³P₁ → ³H₅) [3]. Unexpectedly, it is found that the energy transfer is different toward the d and f states and that the energy transfer toward the d orbitals is strongly affected by the thermal treatment.

This research was supported by project 21AG-1C030 of SCS of RA. EPR studies were supported by project 20RF-024 of SCS of RA and by 20-52-0500 Arm_a of RFFBR.

References

- [1] J. Pejchal, M. Buryi, V. Babin, et al, J. Luminescence 181, 277-285, 2017.
[2] M. Nikl, H. Ogino, A. Krasnikov, et al, Phys. Stat. Sol. (a) 202(1), R4-R6, 2005.
[3] K. Sreebunpeng, W. Chewpradiktul, V. Babin, et al, Radiation Measur. 56, 94-97, 2013.

Poster report

Synthesis and Spectroscopic Properties of YAlO₃:Er Crystals for 1.6 μ m Lasers

M. V. Derdzian¹, K. L. Hovhannesian¹, A. V. Eganyan¹, A. G. Petrosyan¹, K. N. Gorbachenya², V. E. Kisel², A. A. Tarachenko², and N. V. Kuleshov²

¹*Institute for Physical Research, National Academy of Sciences of RA, 0204 Ashtarak-2, Armenia*

²*Center for Optical Materials and Technologies, Belarusian National Technical University, Nezavisimosty Ave., 65, Minsk 220013, Belarus*

Email: mderdzian@gmail.com

Resonantly pumped erbium lasers emitting in the 1.5-1.6 μ m range on the $^4I_{13/2} \rightarrow ^4I_{15/2}$ transition of Er³⁺ ions are under active studies for several applications, such as laser range finding, fiber-optic communication systems and optical location [1].

In the present work YAlO₃:Er (YAP:Er) perovskite is selected for evaluation of its potential. Crystals doped with 0.5-16 at% Er were grown by the vertical Bridgman method. The optimal ratio Y/Al in initial melts was determined with regard to formation of anti-site defects (Y³⁺ ions on Al³⁺ sites or vice versa) leading to non-stoichiometry and separation of secondary phases. Twin and light scatter free, and non-additionally colored crystals 12 mm in diameter and 40 mm long were obtained and characterized.

For spectroscopic investigations in polarized light, plates oriented along crystallographic axes were cut from the YAP:Er crystal. Polarized absorption spectra at room temperature were measured with a spectrophotometer Varian CARY 5000. The spectral bandwidth was 0.4 nm. The absorption spectra of the YAP:Er crystal in the spectral range of 1350–1700nm (transition $^4I_{15/2} \rightarrow ^4I_{13/2}$ of erbium ions) are presented in Figure 1. The highest absorption can be observed at 1515nm for light polarization E//a.

This research was supported by SCS of RA 21SC-BRFFR-1C002, and partially supported by BRFFR F21ARM-004.

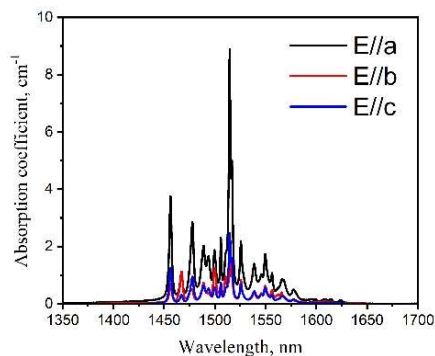


Fig. 1. Absorption spectra of YAP:Er crystal

References

- [1] K.N. Gorbachenya, S.V. Kurilchik, V.E. Kisel, et al, Quantum Electron 46(2), 95–99, 2016.

Investigation of Bremsstrahlung in Electrolyzers with Electrolyte from Ordinary Water

R. N. Balasanyan, I. G. Grigoryan, P. H. Muzhikyan, V. S. Arakelyan, R. B. Kostanyan

Institute for Physical Research of the National Academy of Sciences of Armenia

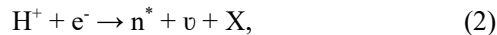
Email: irina.g.grigoryan@gmail.com

The paper [1] presents the physical mechanism for the occurrence of an electrically induced nuclear phenomenon in ordinary water through the structural formation of double electric layers that arise when metal electrodes come into contact with water, in which the formation of quasi-neutrons and, accordingly, the occurrence of nuclear transformations along the $X(n,\gamma)Y$ channel are possible. However, there is no information on the experimental registration of bremsstrahlung of electrons crossing the barrier of the electrical double layer and colliding with hydrogen ions, as a result of which quasi-neutrons are formed along the channel:



where e^- is an electron, n^* is a quasi-neutron, ν is an electron neutrino.

The aim of this work is an experimental study of electrically induced bremsstrahlung of electrons that arise in an aqueous medium in the presence of metal electrodes. This paper presents the results of registration of bremsstrahlung when the electrodes in water are exposed to an electric field with certain parameters.



where X is an X-ray photon with an energy of 5.67 keV, which appears during the deceleration of an electron colliding with a hydrogen nucleus.

It is shown that under the action of an electric field through metal electrodes in water, bremsstrahlung with an energy of 5.67 keV arises. The intensity of X-ray radiation depends on the magnitude of the potential difference and the steepness of the front of the electric signal applied to the electrodes in water. Bremsstrahlung is accompanied by the formation of quasi-neutrons in water and the appearance of nuclear phenomena.

Reference

- [1] Balasanyan R. N.*, Kostanyan R. B. Electrically Induced Nuclear Processes in Electrolyzer. *Physics Journal*. Vol. 2, no. 1, 2016, pp. 45-48.

Gd₃Sc₂Al₃O₁₂:Ce Scintillator Crystals with Ca²⁺, Mg²⁺ and Li⁺ Ions

K. L. Hovhannesyan, M. V. Derdzyan, A. V. Yeganyan, A. G. Petrosyan

Institute for Physical Research, NAS of Armenia, 0203 Ashtarak-2, Armenia

Email: khovhannisyan9@gmail.com

Co-doping of Ce³⁺ activated garnets with impurities of a lower charge than the host cations (Mg²⁺, Ca²⁺, Li⁺) is widely applied to stabilize Ce⁴⁺ states and is efficient to shorten the scintillation decays time important for many future applications [1]. The resulting effect depends on incorporation behavior (site occupation or location at interstitials) and the charge compensation mechanism [2], less understood in the case of Li⁺. The size mismatch and the unit cell volume were considered as most important parameters governing the incorporation behavior of Li⁺.

In this work gadolinium-scandium-aluminum garnet (Gd₃Sc₂Al₃O₁₂ or GSAG) garnet doped with Ce³⁺ (introduced as a scintillator in 1994 [3]) is selected for studies, since the size of Li⁺ (0.76 Å) exactly matches that of Sc³⁺ (0.75 Å) in octahedral coordination and suggests readily substitution for Sc³⁺ sites. The UV absorption profile in Ca²⁺ and Mg²⁺ co-doped GSAG:Ce exhibits a noticeable band at around 250-260 nm which is assigned to the charge transfer absorption of Ce⁴⁺, as observed in several types of garnet crystals. The presence of this band is an indicator for site occupation by the co-dopants with Ce⁴⁺ serving as a charge compensator. In contrast to introduction of divalent co-dopants, no clear evidence for presence of the charge transfer absorption is observed in the case of Li⁺, when taken in moderate quantities. However, this observation is not sufficient to answer on whether Ce⁴⁺ states exist or not in GSAG:Ce, which can be done after additional measurements, e.g. of the scintillation decays. The incorporation behavior of Li⁺, the resulting defect centers and the phase purity of crystals are considered as well for high concentrations of introduced Li⁺.

This work was supported by the State Committee of Science of the Ministry of Education and Science of the Republic of Armenia (project 21AG-1C030).

References

- [1] M. Nikl, K. Kamada, V. Babin, et al, *Cryst. Growth Des.*, **14**, 4827 (2014).
- [2] M.V. Derdzyan, K.L. Hovhannesyan, A.V. Yeganyan, et al, *CrystEngComm*, **20**, 1520 (2018).
- [3] A. Kling, D. Kollwe, D. Mateika, *Nucl. Instr. Meth. Phys. Res. A*, **346**, 205 (1994).

Scattering of a Plane Wave on a Matte Surface

A. Zh. Khachatryan, A. F. Parsamyan

National polytechnic university of Armenian, Teryan 105, Yerevan 0009, Armenia

Email: ashot.khachatryan@gmail.com

In the framework of the present work the reflection of a plane wave from the flat matte surface is discussed. On Fig. 1 the plane wave reflection problem is presented for two types of reflecting surface. First of them it is a flat mirror surface (left Fig. 1) and the second one is a flat matte surface (right Fig. 1).

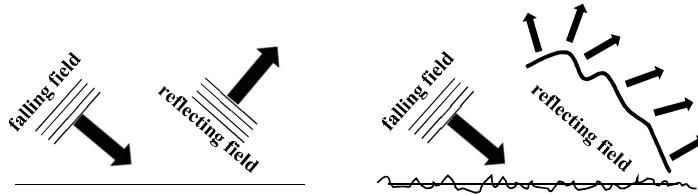


Fig. 1. Reflection of a plane wave from a flat mirror surface (left picture) and from a flat matte surface (right picture).

It is well known that in the case of a flat mirror surface when the falling field is a plane wave the reflected field is a plane wave as well. At the same time, it is obvious that in the case of a matte surface, the shape of the reflected field will have a more complex shape. It is clear as well that the form of the reflected field (the shape of the equiphase surface) will be determined by the degree of roughness of the matte surface. Following Huygens' approach we will consider the reflected field as the result of a superposition of spherical waves generated by the primary wave at points on the reflecting surface;

$$U_{ref}(\vec{R}, t) = \sum_p \frac{a_0}{|\vec{R} - \vec{r}_p|} \cos[\omega t - k|\vec{R} - \vec{r}_p| + \gamma_p], \quad (1)$$

where \vec{R} shows the observation point, \vec{r}_p correspond to points of reflected surface and ω is the frequency of primary (incident) field, which, as it was mentioned, we consider as a plane wave; $U_{inc}(\vec{R}, t) = A \cos(\omega t - \vec{K}\vec{R})$ and $|\vec{K}| = k$. The initial phases of generation of the sphere waves (1) are defined by the locational of the reflected surfaces points in the primary field: $\gamma_p = \vec{K} \cdot \vec{r}_p$. We investigate the sum (1) in the Fraunhofer approximation, when the sphere waves are considered as plane waves [1, 2].

References

- [1] A.Zh. Khachatryan. Armenian Journal of Physics **14**, 201 (2021).
[2] A.Zh.Khachatryan, Zh.R.Panosyan, G.P.Vardanyan, et al. Optik **265**, 169372 (2022).

Using a Focusing Horn to Detect Humans in the Thermal Infrared Region

A. E. Martirosyan¹, V. A. Martirosyan^{1,2}, R. B. Kostanyan¹, P. H. Muzhikyan¹

¹ Institute for Physical Research, NAS of Armenia, Ashtarak-2, 0203, Armenia

² YSU, Faculty of Mathematics and Mechanics, Alex Manoogian 1, Yerevan, 0025, Armenia

Email address: arturmart01@gmail.com

In recent years, thermal infrared (4-14 μ m) sensors have been widely used to detect humans and relatively hot objects. Passive infrared sensors (PIR) usually detect humans at a distance of 6-12 m from the sensor. In [1], object monitoring by a non-matrix detector is carried out without frame-by-frame display technique elaborated by the Lumiere brothers. The gain characteristics of optical conical horns are derived and analyzed in [2].

In this article, we describe the detection system with a conical horn (as an alternative to a lens) as a focusing element and with a thermal infrared sensor. This technique allows one to control the human observation distance and the detection field of view.

When illuminated at a normal angle, the horn's inner surface can be mentally divided into 2 zones: zone *a*, where the incident ray passes the exit window after a single reflection; and zone *b*, where the incident ray passes the exit window after multiple reflections. Theoretical calculations show that conical diameters at the beginning of zones *a* and *b* can be represented as [2]:

$$d_a = \frac{d_0 \sin 3\varphi}{\sin \varphi}, d_b \approx d_0 \cot \varphi,$$

where φ is the cone apex half-angle, d_0 is the diameter of horn's exit window. Note that obtained results are valid if the reflection coefficient of the inner conical surface tends to 1. In the case of homogeneous illumination of the conical horn, the ratio S_b/S_0 shows the magnitude of its gain, where $S_b = \pi d_b^2/4$ is the cross-sectional area of horn at the beginning of zone *b*, and $S_0 = \pi d_0^2/4$ is the area of horn's exit window.

For experimental data acquisition and real-time monitoring of signals from photomultiplier a functional unit consisting of data acquisition board Arduino and laptop with specially developed code in Python programming language are used.

The registration system is applied to detect a human at various distances. The thermal infrared pulse is associated with the appearance of a human in the horn's field of view: the human movement changes the illumination of surrounding local area that is recorded by the detection system. It is shown that using a conical horn as a focusing element allows detecting humans at a much greater distance (up to 25m) than widely used PIR sensors.

References

[1] A.E. Martirosyan, R.B. Kostanyan, P.H. Muzhikyan, *et al.*, *Appl. Opt.* **59**, 7279-7283 (2020).

[2] V.A. Martirosyan, P.H. Muzhikyan, *Appl. Opt.* **60**, 5382-5386 (2021).

Poster report

Formation of Nanostructured Thin Films from Solid-Phase Pyrolysis of Copper Phthalocyanine

S. T. Pashayan¹, H. T. Gyulasaryan¹, A. S. Manukyan¹, S.V. Zlotski², V. M. Anischchik², O. V. Korolik²

¹*The Institute for Physical Research of NAS of Armenia, 0203, Ashtarak-2, Armenia*

²*Belarusian State University, Nezavisimosti Ave., 4, 220030, Minsk, Belarus*

Email: svetlana1207@yahoo.com

One of the main tasks of modern materials science is the development of methods for the manufacture of materials with given structural characteristics that provide the required properties. In recent years, copper nanoparticles (NPs) and thin films have been the object of active research by scientists, which is associated with the possibilities of using them in catalysis, spintronics, biomedicine, in the device of sensors, supercapacitors, solar cells (SC) and other applications. There are various methods for the synthesis of metal NPs and thin films: laser ablation, magnetron sputtering, PLD, chemical vapor deposition, spray pyrolysis, etc. In this study nanostructured thin-film island-type coatings on sapphire and silicon substrates, consisting of copper NPs dispersed in a carbon matrix, were obtained by solid-phase pyrolysis. Polycrystalline powder of copper phthalocyanine was used as a precursor for copper NPs synthesis. The results of the morphological and structural properties of the films obtained are presented in our work.

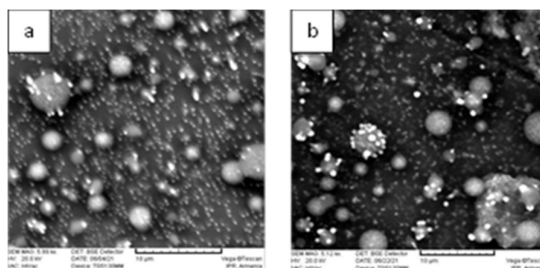


Fig. 1. SEM images of obtained films on sapphire substrate: a - as-deposited ($T_{\text{pir}} = 900 \text{ }^{\circ}\text{C}$, $t_{\text{pir}} = 30 \text{ min}$); b – after annealing ($T=300 \text{ }^{\circ}\text{C}$, $t = 30 \text{ min}$)

The elemental composition, structure and morphology of obtained samples were investigated by SEM, EDX-analysis, AFM, Raman Spectroscopy and X-ray diffraction. The measurements were carried out before and after annealing of the samples (Fig.1). It has been established that the structure, surface properties of the films obtained, as well as the structure of the carbon matrix and the sizes, also vary according to pyrolysis and annealing conditions. The study showed that this method allows to synthesizing NPs, thin-film nanostructures and nanocomposites with desired properties which can be applied in many areas of modern science and technology.

Authors thanks to G. Badalyan for help in SEM measurements.

References

- [1] Díaz, C.; Valenzuela, M.L. et al. Inorg. Chim. Acta, 377, (2011).
[2] Bang, J. H., & Suslick, K. S. Adv. Mat., 22(10), 1039, (2010).

Poster report

Thin Film Field-Effect Transistor with Ferroelectric Channel

N. R. Aghamalyan, H. L. Ayvazyan, R. K. Hovsepyan, Y. A. Kafadaryan,
H.G. Mnatsakanyan, S.I. Petrosyan, A.R. Poghosyan

Institute for Physical Research, Ashtarak-2, Armenia

Email: apoghosyanipr@gmail.com

We present an n-type channel transparent field-effect transistor (FET) using a top-gate configuration. A ZnO:Li ferroelectric film was used as a channel, and a MgF₂ film was used as a gate insulator. A transistor was fabricated on a crystalline sapphire substrate, the channel of which was a sapphire/ZnO:Li/MgF₂ heterostructure. The transistors were fabricated by vacuum electron beam deposition. Textured films with the [001] crystal axis perpendicular to the substrate plane were obtained. Measurements have shown that ZnO:Li films are ferroelectrics with spontaneous polarization $P_s \approx 1\text{--}5 \text{ mC}/\text{cm}^2$ and coercive field $E_c \approx 5\text{--}10 \text{ kV}/\text{cm}$. For 10,000 switchings of spontaneous polarization, this value decreases by 10-15%. The electrical characteristics of a thin-film field-effect transistor were measured: the dependence of the drain-source current I_{DS} on the drain-source voltage U_{DS} at various gate-drain voltages U_{GS} in two antiparallel states of the spontaneous polarization vector. Based on the experimental dependences $I_{DS}=f(U_{DS})$, the values of field-effect mobility and threshold voltage were determined for two states of the spontaneous polarization vector of the ferroelectric channel: a) $\mu = 1.5 \text{ cm}^2/\text{Vs}$, $U_{th} = 30 \text{ V}$; b) $\mu = 1.7 \text{ cm}^2/\text{Vs}$, $U_{th} = 23 \text{ V}$. Thus, switching the spontaneous polarization vector leads to a change in the parameters of the FET channel. Note that UV radiation ($h\nu = 3.2 \text{ eV}$) leads to a decrease in the threshold voltage by 2–3 V in both polarization states, which can be explained by photogeneration of a delocalized hole-electron pair, its displacement and capture at the channel boundary in the dielectric. These results can be used to create a bistable or, more precisely, a digital FET. Based on similar ferroelectric-semiconductor structures, it is possible to create quantum dot field-effect transistors.

Optical Properties of Polarons in Ag-doped ZnO Films

A. Sarkisyan, R. Hovsepyan, N. Aghamalyan, M. Nersisyan, S. Petrosyan, I. Gambaryan,
A. Poghosyan, S. Harutyunyan, Y. Kafadaryan

Institute for Physical Research of National Academy of Sciences, Ashtarak-2, 0203 Armenia

Email: aramasd13@gmail.com

In this work, we report the polaron dynamics in Ag (0.27 at.%) doped transparent zinc oxide films (AgZnO) on a glass substrates as a function of temperature. The optical characteristics of a large-radius polaron and the mechanism of optical conduction based on the Frohlich model are studied. The dynamics of charge switching between localized and delocalized polaron states in AgZnO is considered.

Contents

Massive Matter-Wave Interferometers on the Atom Chip with Nano-Diamonds: a Roadmap	5
R. Folman.....	5
Recent Progress in the Development of Electrically Controllable Lenses and their Applications 5	
Z. Zemska ¹ , P. Larochelle ¹ , T. Galstian ^{1,2,3}	5
Photoionization of Silver: Spectroscopic Research and Application to Radiopharmacy in the SPES – IsolPharm Project Context	6
E. Mariotti ¹ , A. Arzenton ^{1,2} , S. Farracane ² , A. Khanbekyan ¹ , O.S. Kwairakpam ^{1,2} , P. Nicolosi ³ , D. Scarpa ² , A. Andrighetto ²	6
A new Level-Crossing Two-State Model Solvable in Terms of Hypergeometric Functions	9
T. A. Shahverdyan, T. A. Ishkhanyan, and A. M. Ishkhanyan	9
The Gauge Degrees of Freedom in the Theory of the Massless Spin 2 Particle, Solutions with Spherical Symmetry	9
A. V. Bury ¹ , A. V. Ivashkevich ¹ , A. V. Chichurin ² , V. M. Red'kov ^{1g}	9
Electromagnetically Induced Transparency Effect Using Magnetically Induced Transitions: Circular Dichroism Manifestation	10
D. Sarkisyan , A. Tonoyan, and A. Sargsyan.....	10
Spectral and Tuning Characteristics of Extended Cavity Diode Lasers	11
A. P. Bogatov ¹ , A. E. Drakin ¹ , D. S. Chuchelov ¹ , E. A. Tsygankov ¹ , V. V. Vassiliev ¹ , M. I. Vaskovskaya ¹ , V. L. Velichansky ^{1,2} , S. A. Zibrov ¹	11
Femtosecond Lasers in Ophthalmology: Finite Element Modeling of Glaucoma Surgery	12
G. P. Djotyan ^{1,2} , E. R. Mikula ^{2,3} , K. Kranitz ⁴ , Z. Nagy ⁴ , T. Juhasz ^{2,3}	12
Bessel Beam Assisted Photovoltaic Trapping of Micro/nano-objects on a Lithium Niobate Crystal	13
L. Tsarukyan ¹ , A. Badalyan ¹ , L. Aloyan ² , Y. Dalyan ² , R. Drampyan ¹	13
Magneto Plasmon Spectrum in Graphene	14
A. M. Ishkhanyan ^{1,2} , V. P. Krainov ³	14
MacColl-Hartman Paradox Interpretation: a Challenge to the Wave Equation	15
A. Zh. Muradyan.....	15
Atomic Limit in Optical Microscopy & Photon Confinement: Tip-Enhanced Raman Scattering in the Atomistic Near-field	16
V. A. Apkarian.....	16
Preparation and Study of Graphene/LN Heterojunction for Sensorial Application	17
E. Kokanyan ^{1,2} , N. Margaryan ³ , N. Gasparyan ³ , N. Babajanyan ¹	17
Electromagnetically Induced Absorption Resonances in Alkali-Metal Vapor Cells for Applications in Quantum Metrology	18
D. V. Brazhnikov ^{1,2} , V. I. Vishnyakov ¹ , S. M. Ignatovich ¹ , M. N. Skvortsov ¹	18
Simulation of Terahertz Radiation Generation by Femtosecond Pulses Propagating in Nanocomposites with Semiconductor Quantum Dots	19
O. Fedotova ¹ , A. Husakou ² , R. Rusetski ¹ , O. Khasanov ¹ , A. Fedotov ³ , T. Smirnova ⁴ , U. Sapaev ⁵ , P. Klenovsky ^{6,7} , and I. Babushkin ^{8,9,2}	19
Versatile Tools for Manipulating Light Enabled by the 4th Generation Optics	20
N. Tabiryan	20

Simulating Universal Gaussian Circuits with Linear Optics	22
L. Chakhmakhchyan ^{1,2} , N. J. Cerf ¹	22
Shallow Donors in Gapped Graphene Systems	23
A. P. Djotyan, A. A. Avetisyan.....	23
On the Method and Results of Calculation of the Tetrahedral Splittings and Resonance Interactions in Vibrational Spectra of High Symmetry Molecules	24
E. S. Bekhtereva, O. N. Ulenikov, O. V. Gromova, N. I. Nikolaeva.....	24
Generation of Two Entangled Photons During the Decay of a Single Photon in an Optical Fiber with Random Boundaries	24
A. S. Gevorkyan ^{1,2}	24
High Resolution Ro–Vibrational Analysis of Molecules in Doublet Electronic States: the $\nu_1+\nu_3$ Band of Chlorine Dioxide ($^{16}\text{O}^{35}\text{Cl}^{16}\text{O}$) in the X^2B_1 Electronic Ground State	26
O. N. Ulenikov ¹ , E. S. Bekhtereva ¹ , O. V. Gromova ¹ , S. Bauerecker ²	26
Atom-Surface Interaction in a Potassium Nanocell	27
A. Sargsyan, D. Sarkisyan	27
Expanded Ro–Vibrational Analysis of the Dyad Region of $^{12}\text{CD}_4$ and $^{13}\text{CD}_4$: Line Positions, Energy Levels, and Absolute Line Strengths	27
O. V. Gromova ¹ , O. N. Ulenikov ¹ , E. S. Bekhtereva ¹ , S. Bauerecker ²	27
Plasmonic Nanostructures with Laser Induced Chirality	28
I. A. Gladskikh, D. R. Dadadzhyanov, A. Sapunova G. Alexan, R. A. Zakoldaev, T. A. Vartanyan	28
Noise Calculation of Various Design Thermoelectric Detection Pixel for UV Single Photons Registration	29
A. S. Kuzanyan ^{1,3} , A. A. Kuzanyan ^{1,2} , V. R. Nikoghosyan ¹ , S. R. Harutyunyan ^{1,3}	29
Dressed States and Suppression of Dissipative Processes	30
G. G. Grigoryan	30
Polaron Mechanism of Conductivity in Zinc Oxide Films	31
N. R. Aghamalyan ¹ , H. L. Ayvazyan ¹ , R. K. Hovsepyan ¹ , Y. A. Kafadaryan ¹ , H. G. Mnatsakanyan ¹ , A. R. Poghosyan ¹ , T. A. Vartanyan ²	31
Suppression of the Light Shift of the CPT Resonance Frequency in ^{87}Rb Atoms	31
M. I. Vaskovskaya, E. A. Tsygankov, D. S. Chuchelov, S. A. Zibrov, V. V. Vassiliev, V. L. Velichansky	31
Magnetic Field Values Annihilating Alkali Atoms' Transitions	32
A. Aleksanyan ^{1,2} , R. Momier ^{1,2} , E. Gazazyan ^{1,3} , A. Papoyan ¹ , C. Leroy ²	32
Temperature Dynamics of Laser Heating of Composites "Substrate/Amorphous Silicon Film" and "Substrate/Gold Nanoparticles/Amorphous Silicon Film"	34
A. Fedotov, Y. Tsitavets, I. Dadenkov.....	34
Atomic Cells Production by Laser Technology	35
D. S. Chuchelov ¹ , A. B. Egorov ² , E. A. Tsygankov ¹ , V. V. Vassiliev ¹ , M. I. Vaskovskaya ¹ , V. L. Velichansky ^{1,3} , S. A. Zibrov ¹	35
Nanometric-Thin K Vapor Cell Used as a Large-Range Magnetometer	36
R. Momier ^{1,2} , A. Sargsyan ² , A. Tonoyan ² , M. Auzinsh ³ , D. Sarkisyan ² , A. Papoyan ² and C. Leroy ¹ ..	36
Terahertz Generation Using a Nitrogen-Doped Diamond Photoconductive Antenna	37
V. V. Bulgakova ¹ , P. A. Chizhov ¹ , M. S. Komlenok ¹ , V. V. Kononenko ¹ , V. V. Bukin ¹ , A. A. Ushakov ¹ , A. A. Khomich ² , A. P. Bolshakov ¹ , V. I. Konov ¹ , S. V. Garnov ¹	37

An Asymmetric Version of the Second Demkov-Kunike Level-Crossing Model	38
T. A. Shahverdyan ^{1,2} , A. M. Ghazaryan ^{1,2} , and A. M. Ishkhanyan ^{1,2}	38
Combined Method of Laser and Chemical Treatment of Painted Gypsum Base-Relief	38
A. V. Vasileva ¹ , A. K. Kareva ² , V. A. Parfenov ¹	38
Surface Enhanced Raman Scattering by Dye Molecule on Silver Substrates	39
M. Goncalves ¹ , A. Melikyan ² , H. Minassian ³ , P. Petrosyan ⁴	39
Narrow-Band and Bright Fluorescence of Silver Nanoclusters in a Plasmonic Cavity	40
A.S. Gritchenko ¹ , A.S. Kalmykov ¹ , B.A. Kulnitskiy ^{2,3} , Y.G. Vainer ¹ , Shao-Peng Wang ⁴ , B. Kang ⁴ , P.N. Melentiev ¹ and V.I. Balykin ¹	40
Synthesis, Structure, Magnetic and Magnetic Heating Properties of Carbon Coated Fe-Fe₃C Nanoparticles	41
H. Gyulasaryan ¹ , E. Myrovali ² , G. Chilingaryan ¹ , E. Papadopoulou ³ , N. Tetos ³ , A. Ginoyan ¹ , A. Makridis ² , N. Sisakyan ¹ , M. Spasova ³ , M. Farle ³ , M. Angelakeris ² , A. Manukyan ¹	41
Influence of Buffer Gases on the Quality Factor of CPT-Resonance in 87Rb: Ar and Ne vs N₂	42
K. M. Sabakar ^{1,2} , M. I. Vaskovskaya ¹ , D. S. Chuchelov ¹ , E. A. Tsygankov ¹ , S. A. Zibrov ¹ , V. L. Velichanskiy ^{1,2}	42
LiNbO₃:Tm³⁺ Crystal: Material for Radiation Balanced Laser	43
N. Mkhitarian ^{1,2} , G. Demirkhanyan ^{1,2} , N. Kokanyan ^{3,4} , M. Aillerie ³ , E. Kokanyan ^{1,2}	43
Optical Techniques for the Study of DNA–porphyrin Interactions	45
L. Aloyan, Y. Dalyan.....	45
Effect of γ-Irradiation on the Semitransparent Gray Color Obsidian in the 5 to 500 kGy Range	46
N. R. Aghamalyan, I. A. Gambaryan, E. A. Kafadaryan, M. N. Nersisyan, H. T. Gyulasaryan, G. N. Chilingaryan.....	46
Formation of Ce³⁺ Luminescence Bands in YAG:Ce Crystals	46
T. I. Butaeva, K. L. Hovhannesyanyan, A. V. Eganyan, A. G. Petrosyan.....	46
Depth Spectroscopic Analysis of the YAG - Yb³⁺ Ceramics	47
G. Demirkhanyan, ^{1,5} B. Patrizi, ^{2*} R. Kostanyan, ^{1,6} J. Li, ⁴ A. Pirri, ³ Y. Feng ⁴ , T. Xie, ⁴ Zh. Yang, ⁴ M. Vannini, ² M. Becucci, ⁶ D. Zargaryan, ¹ G. Toci ²	47
Investigation of YAG:Pr,Ca Scintillator Crystals Annealed in Air	48
M. V. Derdzyan ¹ , K. L. Hovhannesyanyan ¹ , S. N. C. Santos ² , G. R. Asatryan ³ , C. Dujardin ² , A. G. Petrosyan ¹	48
Synthesis and Spectroscopic Properties of YAlO₃:Er Crystals for 1.6μm Lasers	49
M. V. Derdzyan ¹ , K. L. Hovhannesyanyan ¹ , A. V. Eganyan ¹ , A. G. Petrosyan ¹ , K. N. Gorbachenya ² , V. E. Kisel ² , A. A. Tarachenko ² , and N. V. Kuleshov ²	49
Investigation of Bremsstrahlung in Electrolyzers with Electrolyte from Ordinary Water	50
R. N. Balasanyan, I. G. Grigoryan, P. H. Muzhikyan, V. S. Arakelyan, R. B. Kostanyan.....	50
Gd₃Sc₂Al₃O₁₂:Ce Scintillator Crystals with Ca²⁺, Mg²⁺ and Li⁺ Ions	51
K. L. Hovhannesyanyan, M. V. Derdzyan, A. V. Yeganyan, A. G. Petrosyan.....	51
Scattering of a Plane Wave on a Matte Surface	52
A. Zh. Khachatryan, A. F. Parsamyan.....	52
Using a Focusing Horn to Detect Humans in the Thermal Infrared Region	53
A. E. Martirosyan ¹ , V. A. Martirosyan ^{1,2} , R. B. Kostanyan ¹ , P. H. Muzhikyan ¹	53

Formation of Nanostructured Thin Films from Solid-Phase Pyrolysis of Copper Phthalocyanine	54
S. T. Pashayan ¹ , H. T. Gyulasaryan ¹ , A. S. Manukyan ¹ , S.V. Zlotski ² , V. M. Anischchik ² , O. V. Korolik ²	54
Thin Film Field-Effect Transistor with Ferroelectric Channel	55
N. R. Aghamalyan, H. L. Ayvazyan, R. K. Hovsepyan, Y. A. Kafadaryan, H.G. Mnatsakanyan, S.I. Petrosyan, A.R. Poghosyan.....	55
Optical Properties of Polarons in Ag-doped ZnO Films	56
A. Sarkisyan, R. Hovsepyan, N. Aghamalyan, M. Nersisyan, S. Petrosyan, I. Gambaryan, A. Poghosyan, S. Harutyunyan, Y. Kafadaryan	56